Copyright Warning & Restrictions

The copyright law of the United States (Title 17, United States Code) governs the making of photocopies or other reproductions of copyrighted material.

Under certain conditions specified in the law, libraries and archives are authorized to furnish a photocopy or other reproduction. One of these specified conditions is that the photocopy or reproduction is not to be "used for any purpose other than private study, scholarship, or research." If a, user makes a request for, or later uses, a photocopy or reproduction for purposes in excess of "fair use" that user may be liable for copyright infringement,

This institution reserves the right to refuse to accept a copying order if, in its judgment, fulfillment of the order would involve violation of copyright law.

Please Note: The author retains the copyright while the New Jersey Institute of Technology reserves the right to distribute this thesis or dissertation

Printing note: If you do not wish to print this page, then select "Pages from: first page # to: last page #" on the print dialog screen

ABSTRACT

BEHAVIOR OF HUMAN DERMAL FIBROBLASTS SEEDED ON A SILICON MEMBRANE UNDER APPLIED MULTI-AXIAL MECHANICAL FORCES
by

Laura Osorno

The main objective of this thesis is to understand, from a molecular perspective, the morphological and functional abnormalities of human dermal fibroblasts as a response to deformation produced by a normal force that can lead to the potential formation of stretch marks in pregnant women, adolescents, and people with Cushing's syndrome. The main function of dermal fibroblasts is to produce the essential fibrous components of the extracellular matrix (ECM) of the skin.

In order to study the mechanism of stretch mark formation, neonatal human dermal fibroblasts were seeded on a silicon membrane for controlled deformation. Upon reaching a confluence of 40-70%, they were multi-axially stretched using a device designed specifically for this thesis. A total of three samples were analyzed; two samples were exposed to 20% static strain for a time period of one hour and one sample for 24 hours.

The cells presented severe morphological changes after stretching the membrane. They acquired a rounded morphology with unclear cytoplasm and nucleus. Also, the cells started to move throughout the membrane.

It has been shown that dermal fibroblasts show significant morphological changes when subjected to deformation. The observed changes are a result of total strain. Future experiments will focus on improving the device for longer periods of cell deformation and for protein synthesis.

BEHAVIOR OF DEFORMED DERMAL FIBROBLASTS SEEDED ON A SILICON MEMBRANE UNDER HIGH LEVELS OF STRAIN

by
Laura Osorno

A Thesis
Submitted to the Faculty of
New Jersey Institute of Technology
and Rutgers, The State University of New Jersey – Newark
in Partial Fulfillment of the Requirements for the Degree of
Master of Science in Biomedical Engineering

Department of Biomedical Engineering

May 2015

APPROVAL PAGE

BEHAVIOR OF DEFORMED DERMAL FIBROBLASTS SEEDED ON A SILICON MEMBRANE UNDER HIGH LEVELS OF STRAIN

Laura Osorno

Dr. Michael Jaffe, Thesis Advisor — Date
Research Professor of Biomedical Engineering, NJIT

Dr. Bryan J. Pfister, Committee Member — Date
Associate Professor of Biomedical Engineering, NJIT

Dr. Treena Arinzeh, Committee Member — Date
Professor of Biomedical Engineering, NJIT

Dr. Bozena Michniak-Khon, Committee Member — Date
Professor of Pharmaceutics, Rutgers University, New Brunswick and
Director of the Center for Dermal Research

Mr. Norman Richardson, Committee Member — Date
BASF – The Chemical Company, Tarrytown, NY

BIOGRAPHICAL SKETCH

Author: **Laura Osorno**

Degree: Master's Degree

Date: May 2015

Undergraduate and Graduate Education:

- Master of Science in Biomedical Engineering,
  New Jersey Institute of Technology, Newark, NJ, 2015

- Bachelor of Science in Biomedical Engineering,
  New Jersey Institute of Technology, Newark, NJ, 2014

- Applied Science Associates in General Engineering,
  Union County College, Cranford, NJ, 2011

Major: Biomedical Engineering

This thesis is dedicated to those who believe that with hard work and perseverance everything can be achieved.

ACKNOWLEDGMENT

First and foremost, I would like to thank God for having given me the opportunity to complete this thesis. Thanks to Dr. Michael Jaffe for being the chair of my committee and for providing the materials to build the stretching device. Special thanks to Dr. Bryan Pfister, committee member, for his unconditional support, inputs, and guidance during the completion of this work. Thanks to him, I was able to use the lab facility as well as the materials needed in order to execute the experiments and collect proper data. Thanks to Dr. Michniak-Khon for providing me neonatal human dermal fibroblasts and to Mr. Roman Richardson from BASF for his academic support. Thanks to Dr. Roman for his help running the ANSYS simulation of the deformation of the membrane. With the help and technical support of John Hoinowski and Dr. Zohar Ophir, I was able to build and design the stretching device.

I would like to specially thank Alexandra Adams who taught me the different lab techniques used to execute the experiments. Although her project was not related to mine, she took the time to help me and to answer my questions. The time I spent with Alexandra Adams in the lab was full of new experiences which made me mature both emotional and professionally, making me realize how much I can learn from others.

I am grateful at the effort my parents, Olga Londono and John Osorno, have been making in order to see me grow and become the responsible and perseverant woman I am today. I thank them for their time, love, and emotional support. I am especially thankful for the emotional support of a very special person, Juan F. Ceballos. He gave me the initial idea of the topic of this thesis.

TABLE OF CONTENTS

TABLE OF CONTENTS
(Continued)

Chapter **Page**

LIST OF TABLES

LIST OF FIGURES

TABLE OF FIGURES
(Continued)

TABLE OF FIGURES
(Continued)

CHAPTER 1

INTRODUCTION

1.1 Objective

The objective of this dissertation is to model the mechanism of skin stretching by a normal force as observed in pregnancy, weight gain, use of skin expanders for cosmetic reconstruction, and muscle growth during adolescent and weight lifting. A multi-axial stretching device was designed as a model to understand, from a molecular perspective, how high mechanical forces influence dermal fibroblast's behavior leading to fibroproliferative disorders such as mild dermal scars (stretch marks) or pathologic scars. It is hypothesized that these cells undergo morphological and functional changes when they are exposed to high levels of strain at critical strain rates [1]. Based on literature finding, high mechanical forces inhibit dermal fibroblasts from producing the essential fibrous components mainly collagen [2-4]

1.2 Definition of a Scar and How They are Formed

Scarring is known as the end result of the entire wound healing process characterized by fibroproliferative disorders and fibroblast dysfunction[5-7]. It is considered as a morphogenetic problem because of "the failure of the regeneration of the normal skin structure" [6]. In most cases, it occurs after trauma, injury, surgery, [6] or excessive stretching of the skin as in pregnancy, weight gain, muscle gain, and/or the use of skin expanders for breast reconstruction.

The wound healing process is divided into three phases: inflammatory, proliferative/tissue formation, and maturation/remodeling. Homeostasis takes places during the inflammatory phase through the activation of the coagulation cascade, complement cascade, and platelet activation. This occurs in order to prevent loss of blood as well harmful pathogens to enter. Active mediators, such as TGF-β, are released as the inflammatory cells migrate into the wounded area. It is believed that TGF-β has a significant role in scar development. Fibroblasts then start migrating; as they differentiate into myofibroblasts, they secrete collagen fibers, mainly type III collagen observed in immature scars, and type I collagen in mature scars. The collagenous ECM is known as granulation tissue which replaces the initial fibrin scab or blood clot [8, 9].

The remodeling phase is characterized by the continuous synthesis and breakdown of collagen as the ECM remodels. The degradation of collagen is achieved by specific enzymes known as metalloproteinases (MMPs) which are produced by fibroblasts. "The synthesis and secretion of [MMPs] is regulated by growth factor, cytokines, and phagocytic stimuli."[10]. The most common type of MMP is known as matrix metalloproteinase 1 (MMP1) or interstitial collagenase because their function is to degrade collagen types I, II, and III. In general the activity of MMPs is well regulated because they have the potential of degrading the ECM fibrous components, thus impairing the healing process.

Metalloproteases are enzymes (proteins) that use a metal (zinc) to carry out their catabolic reactions. MMP1 is a subfamily of the metalloproteinase group. The presence of MMP1s is commonly observed in processes such as: tissue repair, chronic cutaneous

ulcers, and malignant tumors. It is believed that growth factors, cytokines, physical stress, cell-cell and cell-ECM interactions activate the production of such proteins [1].

It has been demonstrated that high magnitudes of stress/strain exerted on skin fibroblasts activate the over-production of MMP1s [1], and decrease the synthesis of collagen. Some of the most drastic consequences of collagen fragmentation are: disassembly of the actin cytoskeleton of the dermal fibroblasts, reduction in cell spreading, and reduction in collagen synthesis, [11]. According to Xia et al., the mechanical properties and the functionality of the dermis are compromised by the catabolic function of MMP1s, preventing the fibroblasts from adhering to the collagen fibers. As a consequence, the architecture of the skin is overexposed to improper healing [11].

Alterations, interruptions, aberrancies, or prolongation in one or more of the wound healing phases can cause improper or impaired tissue repair. Wounds with the characteristics of impaired healing, like delayed acute wounds or chronic wounds, enter a state known as pathologic inflammation [4]. The main factors that influence wound healing are:

- Inadequate blood supply
- Increased skin tension
- Infections
- Age
- Glucocorticoid steroids
- Obesity
- Alcohol consumption
- Smoking
- Nutrition

1.3 The Different Types of Scars

There are several different types of scars are they are all classified as fibroproliferative disorders[12]. This thesis will only focus on three:

a. **Keloid scars:** type of hypertrophic scar that occurs on areas with high tension. It has been suggested that keloids formation involves a genetic predisposition since there have cases reporting the formation of keloids on the mid-chest in the absence of any injury. Keloids tend to extend beyond the initial site of injury. Keloid scars are characterized by their pink or purple tumor-like shaped with a shiny surface containing disorganized, thick type I and III collagen bundles. [13]

b. **Hypertrophic scars:** these scars are characterized for not extending beyond the initial site of injury. They usually occur because of wound infection or wound closure with excess tension. Hypertrophic scars are commonly red, linear, and nodular with wavy type III collagen fibers oriented parallel to the epidermis surface with nodules and myofibroblasts.[13]

c. **Stretch marks:** also known as striae distensae (SD) are considered a type of scarring of the skin characterized by a change in color based on their stage. They are caused by tearing of the dermis, produced by continuous and progressive mechanical stretching of the skin, presence of high concentration of steroid hormones, and rapid increase in size of particular regions of the body. SD are sometimes considered as an indication of a pathological condition of the connective tissue due to loss of synthetic capacity of fibroblasts. [14, 15]

1.4 Current Trends in Skin Care Industry for Treating Scars

Dermal scars are commonly treated with topical creams containing active ingredients to either maintain or improve the dermis structure. In order to help minimize the appearance of dermal scars, the molecular environment should be optimally stimulated. Substances such as *Centella Asiatica*, rose hip oil, and hydroxyprolisilane-C provide amino acids (hydroxyproline and aspartic acid) that help with the regeneration of the fibrous components of the skin. [7]

Current scar treatments to minimize the appearance of scars, include the use of: "sunscreen, scar massage, hydration ointments and dressings, adhesive microporous

hypoallergic paper tape, silicone gel ... pressure dressings, vitamin E and D, and Mederma®,, [8]. Mederma® aids in scar minimization by reducing inflammation because of its active ingridients such as, allium cepa, an onion extract, and the molecule Quercetin, which is an anti-inflammatory. [8]

Other treatments like the silicon sheeting reduce the risk of abnormal scar formation if used daily for more than twelve hours, for a period of three to six months. If a moist exposed burn ointment and/or a silicone gel is used while using the silicon sheeting, the appearance of the scar is improved since moisture is maintained. The special ingredients of the moist exposed burn ointment, for instance, β-sistosterol and six herbal extracts, help retain moisture. [8]

Treatment for stretch marks has always been challenging since the exact origin and development is poorly understood. In order to treat stretch marks, it is necessary to start at the early or active stage before the scarring process is complete. Different topical therapies, laser, microdermabrasion, and other specialized treatments have been used in the aims to eliminate stretch marks. However, there is nothing that successfully has worked. The following is a short summary of the most common treatments:

- **Tretinoin:** vitamin A derivative. It has been demonstrated that using this product improves the medical appearance of stretch marks when used during their early stages. Treated stretch marks had a decrease in dimensions, 14% length, and 8% width. [15]

- **Centella asiatica extract:** prevents stretch marks development during pregnancy. It stimulates fibroblastic activity and acts as a constraint against glucocorticoids. [15]

- **Pulsed-Dye Laser (PDL):** most commonly used laser treatment to improve the appearance of stretch marks. It is recommended to be used at the early stage of stretch marks because of the blood vessel dialation. This method uses 585-nm flashlamp PDL therapy using dynamic cooling. It has been shown that this type of treatment increases the deposition of collagen in the extracellular matrix. [15]

CHAPTER 2

BACKGROUND AND SIGNIFICANCE

In Chapter 2, the background and the significance of preventing dermal scars is reviewed. Also, the normal physiology of the skin is compared to stretched skin in order to explain and differentiate normal skin from stretched skin, and perhaps to understand the potential origin of dermal scars.

2.1 Rationale

According to the American Society of Plastic Surgeons [16], scar revision surgeries are among the top five reconstructive procedures in the US in 2013. They had an increment of 4% from 2012, leaving a total of 177,317 reported cases. In 2014, 14.6 million cosmetic plastic surgery procedures were performed including breast augmentation implants, abdominoplasty, face-lifting, among other surgeries which are all prone to leave scars on the patient's skin. [16]

An estimated 100 million people worldwide develop scars every day: "11 million keloid scars, 4 million burn scars" [5], "70% of adolescent girls and 40% of boys" [17] and 90% of pregnant women develop stretch marks [17]. These statistics demonstrate the current need of more in depth research on dermal scars formation. Nowadays, dermal scars are a common cause of consultation for dermatologists. In general, scars can be disfiguring and aesthetically unpleasant causing severe itching, pain, sleep disturbance, anxiety, depression, and disruption in daily activities. Therefore, patients are in great need of a guaranteed and effective treatment. [5, 14]

As of today, there are no treatments that either prevent the formation of dermal scars or eliminate them. According to Ferguson et al., "current treatments are empirical, unreliable and unpredictable" [6]. Nowadays, many people and companies focus their experimental methods on using animals such as rodents to analyze the wound healing process and come up with new strategies and therapies that will be used by humans. However, using these animals for such purposes is not ideal because of the differences between the physiology and wound healing process between rodents and humans.[18] New techniques such as using engineered devices, decellularized matrix to grow skin, collagenous matrix or other scaffolds, among other elements could be better used to come up with new therapies for the prevention of dermal scars [18]. For instance, "The development of novel dressings and scaffolds … can be incorporated … to indicate the healing status of a wound or to deliver bioactive molecules or cells to the wound" [18]. Furthermore, new research is needed in order to understand how dermal fibroblasts are affected by high multi-axial forces and hormones in order to have a basic insight in the molecular changes present during dermal scar development.

2.2 Normal Skin vs Stretched Skin

The skin is considered the largest organ in the body, constituting 16% of total body weight [20]. Its main function is to act as a protective barrier keeping foreign agents from coming into the body. In order for skin to maintain its healthy structure, it needs mechanical support, which is provided by the extracellular matrix (ECM) [21].

When a constant mechanical stress is applied to skin, two different phenomena occur: at tissue level, the skin is loaded with tension causing a change in thickness, and producing both mechanical creep and biological creep are observed. Mechanical creep consists on morphological changes at a cellular level; whereas biological creep refers to the disruption of gap junctions, and an increase in tissue surface area which stimulates cell proliferation. The growth of more tissue restores the resting tension of the stretched skin back to normal skin [22, 23]. At the cellular level, mechanotransduction takes place, affecting cytoskeletal rearrangement, protein kinases, and growth factors [23].

2.2.1 Anatomy and Physiology of the Skin

The skin is composed of three main layers: epidermis, dermis, and hypodermis.

The epidermis "is a terminally differentiated squamous epithelium" [20] with keratinocytes as its major cell type. Keratinocytes synthesize keratin, and in the event of injury, they produce cytokines as an immediate response. The dermis is located between the epidermis and a layer fat known as they hypodermis. The thickness of the dermis usually varies between 1mm to 5 mm, depending on the area of the body. The main function of the dermis is to act as a specialized structure protecting the body against mechanical injury. The main components of the dermis are polysaccharides and proteins,

and the major cell type is fibroblasts which are in charge of the production of collagen and elastin fibers and the maintenance and repair of healthy connective tissue. In the dermis, 75% is collagen type I and 15% is collagen type III composing a total of 30% of the total volume of the dermis. Elastin fibers provide the skin its elastic framework, and collagen fibers are responsible for the mechanical strength of the skin [9, 20]. The hypodermis is the innermost layer of the skin. It is composed of cell specialized in storing fat known as adipocytes. The hypodermis acts as an energy reserve and helps in temperature regulation [24].

Figure 2.1 is a schematic representation of the skin layers and their proper function of each of the different parts of the skin:

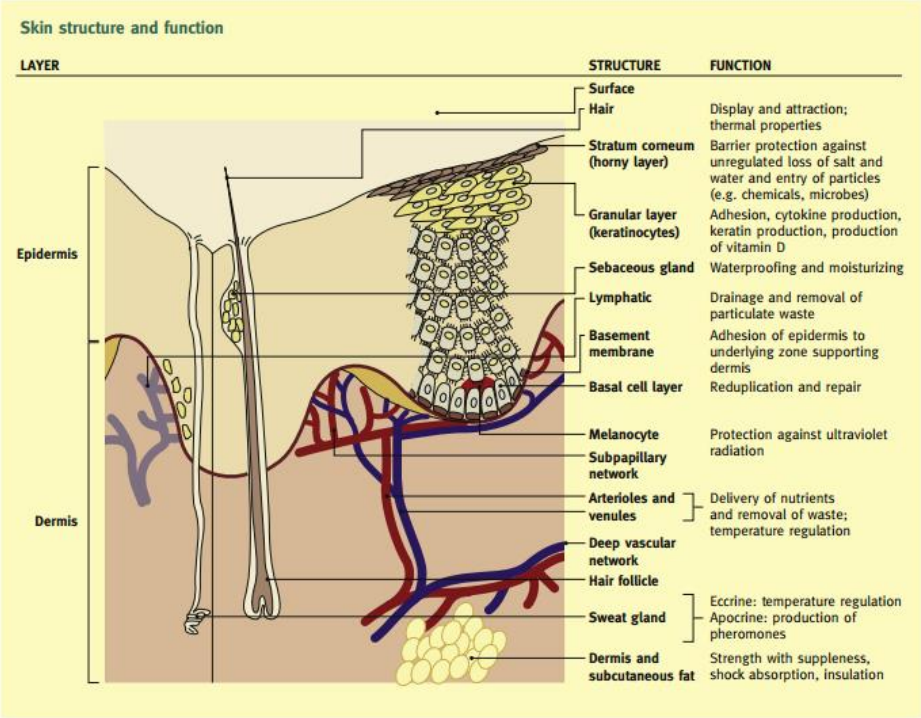

Figure 2.1: Schematic representation of the skin layers and the different parts that compose the skin as the largest organ.

Source Venus M, Waterman J, McNab I. Basic physiology of the skin. Surgery (Oxford). 2011;29;10:471-4.

2.2.2 Fibroblasts: The Major Cell Type of the Dermis Layer of the Skin

Dermal fibroblasts are the major and least specialized cell type found in the dermis of the skin. Their main functions are: to produce the architectural framework of the skin (non-rigid extracellular matrix) rich in collagen type I and III, and to assist and support in the repair mechanisms during wound healing. [21]

In general, fibroblasts are morphologically diverse, and their morphological appearance is determined by their location and activity. For instance, in the event of injury, fibroblasts acquire contractile characteristics migrating into the wound in order to synthesize large amounts of collagen, forming a matrix, and helping in the primary isolation and repair of the tissue. In different regions of the body, fibroblasts present different characteristics and react differently to external stimuli. For example, cultured dermal fibroblasts do not present the same plasticity as in-vivo, since they form flat monolayers in culture [25]. That is, in injury, dermal fibroblasts change their actin skeleton gene expression, acquiring contractile properties like smooth muscle cells. The main reason for this transformation is to bring the edges of the wound together. The transformed cells are known as myofibroblasts [21].

Fibroblasts are large, flat, spindle-like cells with an elliptical or elongated nucleus and thin cytoplasm. The nucleus has a delicate membrane and small amount of granular chromatin. There are morphological differences between young and old fibroblasts: young fibroblasts have an irregular branched cytoplasm; the nucleus is ovoid, large, and pale; the cytoplasm is rich in rough endoplasmic reticulum (RER), and the well-developed Golgi complex is located close to the nucleus. The young fibroblasts are actively engaged in protein synthesis to repair and maintain the connective tissue

architecture. As fibroblasts become old, they become inactive and the production of proteins decreases, although they maintain their spindle-like shape. Their nucleus becomes darker and smaller, and their cytoplasm becomes more acidic because of the granular endoplasmic reticulum [25].

Huang et al. hypothesize that scars mostly develop in areas subjected to high stretching tension. The high mechanical forces activate a process known as mechanotrasduction. As a result, fibroblasts and collagens accumulate at the areas of greatest tension, which are more prone to the development of dermal scars, especially hypertrophic scars or keloids. Scars in general can undergo chronic contraction or post-surgical recurrence; and they can also become a psychological burden for those whose scars are visible [1].

2.2.3 Mechanotransduction

Regardless of the amount and magnitude of the force applied to the skin, cells, whether young or old, sense the mechanical forces as a stimuli, and properly respond to it. Mechanotransduction is the process by which the cells convert mechanical stimuli into biochemical stimuli leading the cells to respond. Parts of the cell such as stretch-activated ion channels, integrins, cadherins, growth factor receptors, myosin motors, and cytoskeleton filaments are responsible for the mechanotrasduction process [26]. Altoguh the development of scars is still not well understood, mechanical stimuli cause certain behavior in cells like: adhesion, migration, survival, proliferation, angiogenesis, apoptosis, among others [27]. According to Ogawa et al., cellular stretch can produce different cell responses. For instance, stretched cells can up-regulate epidermal

proliferation and angiogenesis; and, cyclical stretched skin cells express more growth factors than statically stretched skin [27].

In connective tissue, mechanical forces are needed in order for cells, in this case fibroblasts, to differentiate and/or produce extracellular matrix components. In the absence of mechanical forces, connective tissues suffer atrophy. On the other hand, excess load can induce hypertrophy resulting in high strains that cause inflammation, degradation, and apoptosis [27]. The mechanotransduction phenomenon causes contact-dependent cell signals where the cells need to be in a direct cell-to-cell contact [27].

The starting step of the mechanotrasduction pathway is the proper binding of the cell to the ECM through cell surface receptors. Integrin receptors located on the cell surface directly bind to fibronectin, transmitting forces into the cytoskeleton. Thus, actin proteins become activated through conformational changes [27]. Once integrin is activated, its ligands from the ECM bind to it with high affinity, "clustering into focal adhesions with rapid tyrosine phosphorylation" [27]. As a consequence, the cytoskeletal proteins rearrange, activating the Rho GTPase activity, which affects the reorganization of actin proteins. Thus, the cell responds based on these conformational changes [27].

A relatively different pathway gets activated during skin repair and scarring. Some of the signaling pathways activated are: "transforming growth factor β/Smad, integrin, mitogen-activated protein kinase and G protein, tumor necrosis factors α/nuclear factor-kB, Wnt/β-catenin, interleukin, and calcium ion pathways"[27]. For instance, integrin expression and activity can be controlled by tetraspanins or cell sulfate proteoglycans which are known transmembrane proteins [27]. There is a conformational change that results in the unmasking of receptors that activate the TGF-B signaling pathway when

TGF-B bids to alpha-vb8 complex which is seen in wound epithelium and in chronic wounds. The signaling pathway then presents the complex to the membrane-bound MMPs, activating the proteolytic functions of the MMPs [27].

2.3 Mechanical Properties of the Skin

Skin is behaves as both an isotropic and as a viscoelastic material. Its elasticity varies depending upon the direction of the applied force. The usual skin response to stretch is non-linear. The linear effect of stretch is produced by the alignment of the elastin fibers in the dermis. As the load increases, the non-linear effect takes place, and it is produced by the reorientation of collagen fibers and displacement of ECM [28]. According to Edsberg et al., "collagen will fracture at 10 percent elongation, [and] elastin will not fracture until 100 percent extension of its original length is attained" [29]. Figure 2.2 is a stress-strain curve containing the non-linear deformation as mentioned in the previous sentences.

As skin expands, the deformation effect is time-dependent. Both creep and stress relaxation are observed. Creep happens when a constant force is slowly applied, resulting in hyperplastic deformation. Stress-relaxation is characterized by a decrease is tension since skin is maintained at a constant length. Very rapid stretch, as in pregnancy or normal adolescent development, ruptures the collagen fibers, leading to dermal injury.

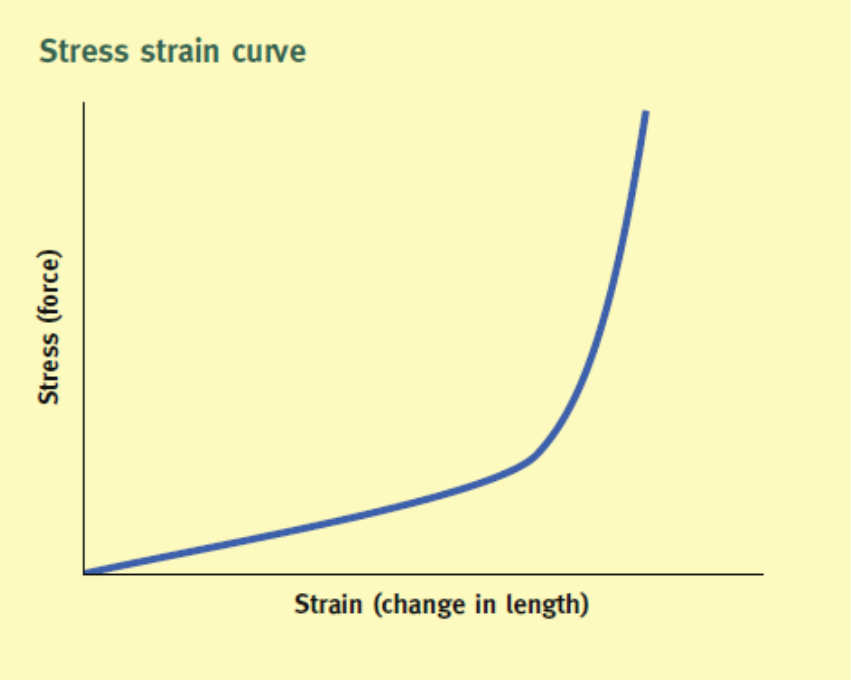

Figure 2.2 Stress-Strain curve of skin.

Source Venus M, Waterman J, McNab I. Basic physiology of the skin. Surgery (Oxford). 2011;29;10:471-4.

CHAPTER 3

MULTIAXIAL STRETHING DEVICE

Stretching both soft tissue and cells has mainly been done in a uniaxial direction in vitro. Since more research needs to be done in a multiaxial direction [1, 30, 31], a stretching device was specifically designed and assembled as part of this thesis as a model to mimic stretching of the skin. The main purpose of building this device was to have a uniform control of high strain levels and time duration, normally applied to either skin samples or dermal fibroblasts cultured on a silicon membrane. This thesis only includes the results from stretching neonatal human dermal fibroblasts at a strain of 20% for a duration of one hour.

3.1 A Review of the Different Stretching Devices

The majority of soft tissue stretching devices have been designed for uniaxial stretch [31-34]. Wang et al.'s stretching device works through the application of a vacuum extending the membrane in the x and y directions. NIH 3T3 fibroblasts were uniaxially stretched to: 16, 26, and 32%. After recording the state of the stress fibers, they observed that "uniaxial stretch led to actin cytoskeleton alignment perpendicular to the direction of stretch" [34]. In addition, Kanazawa et al. used human skin fibroblasts and applied uniaxial cyclical stretch to 20% of the original cell length, at a frequency of 0.16Hz. As a consequence, the cells presented down-regulation of both collagen production and connective tissue growth factor (CTGF). The CTGF plays a key role in the wound healing

cascade since it stimulates cell proliferation, adhesion, chemotaxis, angiogenesis, and production of ECM components. [35]

Huang et al. used an apparatus which applies continuous uniaxial sinusoidal stretch at 10 cycles per minute; they evaluated "the morphological and functional effects of cellular stretch on normal human dermal fibroblasts (hDFs)." [1] Some of their observations are: cells aligned perpendicular to the direction of stretch, and cells increased Matrix-Metalloproteinase (MMP) expression. MMPs are proteins in charge of degrading collagen and other components of the extracellular matrix (ECM). [1]

By contrast, Morrison III et al. used a multi-axial device that allowed the precise control over the mechanical stimulus by independently regulating the strain, strain duration, strain rate, among other parameters. They were interested in studying the mechanical response of brain tissue upon the application of mechanical strain [30]. The silicon "membrane was deformed by a pressure acting normal to the deformed surface"[30]. The basic idea for the stretching device used for this thesis was obtained from Morrison III et al.'s publication

The closest model available in industry of deformation by a pressure acting perpendicular to the surface is the skin expander used for breast reconstructive surgery and for foreskin treatments [22, 23, 36]. On a molecular/cellular level, the skin is loaded with tension after the device is implanted. As a consequence, several integrated cascades, such as the mechanotransduction pathway, the wound healing cascade, among others, are activated leading to the production of skin growth factors, cytokines, proteins, and changes in the cytoskeleton of cells [22, 23]. If the mechanical forces that contribute to skin

growth are not well controlled, either stretch marks will develop or the dermis will rupture[29].

3.2 Design Criteria, Materials, and Methods

The stretching device designed for this thesis differs from Morrison III et al's in the following ways: the multi-axial stretching device is a model to simulate severe stretching of the skin as observed in pregnancy, weight gain, use of tissue expanders, among other conditions. The materials used to build the stretching device were selected based on humidity resistant properties, allowing the device to be placed into the incubator at 37 °C, 5% CO_2, and 95% humidity. The device is composed of two plates (bottom and top), a rounded tip indenter designed to deform the silicon membrane, a mechanical jack which moves the indenter vertically to deform the membrane, a specially designed cell culture well where the silicon membrane is attached and sealed in place using a silicon O-ring, and a cell culture well holder to prevent further movement and misplacement of the culture well.

The Aluminum top plate (Figure 3.1) is designed as a base for the PEEK cell well (Figure 3.3). The well is then held in place with the Aluminum cell well holder as observed in Figure 3.5. The well design was taken from Dr. Pfister's original design, the only difference is that the height of the well was modified in order to hold more cell media, because the device allows for long periods of deformation. Like Dr. Pfister's design, "the well … allow[s] for rapid assembly by press-fitting" [37] the rings together. In between the two PEEK rings, there is an O-ring, which serves three purposes: "1) applie[s] pre-stretch to the silicone membrane, 2) [holds] the well together, and 3) act[s]

as a gasket to prevent media leakage"[37]. The circular shape of the well allows for equibiaxial and uniform tension along the membrane.

The spherical tip indenter deforms the membrane in a tent-like shape. At the very center of the membrane, the strain value can be calculated experimentally, and it can be confirmed using the formula from Morrison III et al's publication [30]. The formula is:

$$\epsilon = \frac{2}{3}\left(\frac{w}{a}\right)^2 - \frac{2}{15}\left(\frac{w}{a}\right)^4 + \frac{2}{35}\left(\frac{w}{a}\right)^6 \tag{3.1}$$

where *w* is the vertical displacement and *a* is the radius of the clamped membrane (10 mm). Since the vertical displacement used for this thesis (5 mm) is greater than half the thickness of the membrane (0.127 mm), the deformation of the clamped-edge circular membrane follows the large-deflection theory which considers both the bending and membrane actions [38].

According to Ansel C. Ugural, "the compressive stresses at the top of the plate may be larger than the tensile stresses at the bottom" [38], which leads one to conclude that the strain distribution on the silicon membrane is not uniform. As previously mentioned, the silicon membrane deforms in a tent-like shape, and equations and analysis of circular membranes following the distributed load theory deformation cannot be used for these experiments. Therefore a new equation must be derived for this type of structural deformation.

A Finite Element Analysis (FEA) was conducted in order to start characterizing the membrane deformation. To execute the FEA, the parameters from Table 3.1 were used. The values of both the Young's modulus and the Poisson's ratio were obtained from

the company, but the value of the Young's modulus is of the material used to make the silicon film, and not the silicon sheet.

Table 3.1 Parameters used to execute the FEA using ANSYS

Parameters used to execute the FEA	Value
Young's modulus	2.6 MPa
Poisson's ratio	0.499
Membrane deflection	5 mm
Load applied to the center of membrane	12,276 Pa
Membrane thickness	0.127 mm

In order to find the value of the applied load, equations from the large-deflection theory were used [38]. First, Equation 3.2 was used to find the flexural rigidity (D) of the Silicone film. Then, Equation 3.3 was used to solve for the pressure load (P) needed for a 5 mm membrane center deflection (Equation 3.4). The values of the Young's modulus (E), the membrane thickness (t), the Poisson's ratio (v), and the membrane deflection (w) are in Table 3.1.

$$D = \frac{Et^3}{1 - v^2} \tag{3.2}$$

$$\frac{Pr^4}{64Dt} = \frac{w}{t}\left[1 + 0.65\left(\frac{w}{t}\right)^2\right] \tag{3.3}$$

$$P = \frac{64Dt}{r^4}\frac{w}{t}\left[1 + 0.65\left(\frac{w}{t}\right)^2\right] \tag{3.4}$$

The theoretical results of the membrane deformation were compared to the results obtained using ANSYS (Figure 3.1). Based on Equation 3.4, a pressure load of 12,276 Pa

and a deflection to thickness ratio of 50 are needed for a 5 mm membrane deformation at the center. The results from ANSYS match the theoretical results, because the same amount of pressure is needed for a 5 mm deflection. The deflection to thickness ratio varies from the theoretical value. However, this difference is not significant for this thesis.

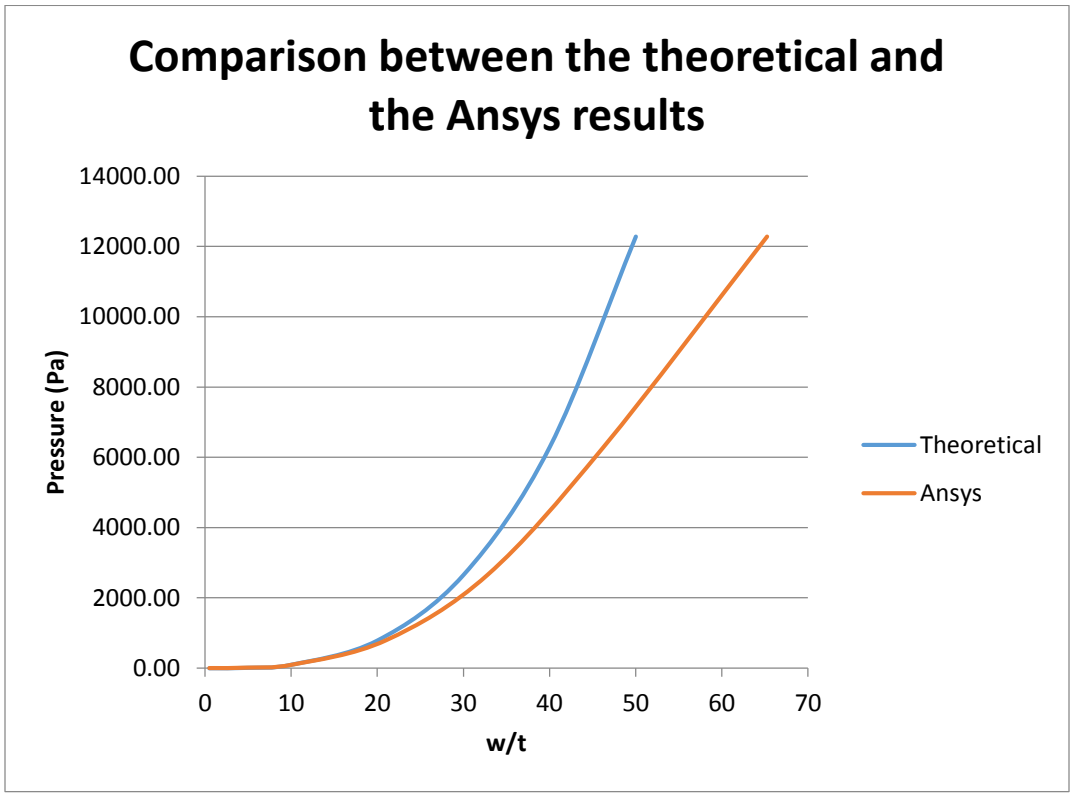

Figure 3.1 Comparison between theoretical results and ANSYS results.

In addition, a tensile test of the silicon sheet was conducted in order to verify the actual Young's modulus of the film. After conducting the tensile test, the results present differences between the experimentally obtained Young's modulus and the one obtained from the company. The difference lies in that the Young's modulus provided by the company is of the material used to make the films at 200% deformation, whereas, the Young's modulus from the tensile test was obtained at 100% deformation. The Young's modulus obtained directly from the company was used for the calculation of this thesis.

Figure 3.2 is the stress-strain curve experimentally obtained from the tensile test of five silicon sheet samples. The average Young's modulus value from the tensile test at 100% deformation is 1.26 MPa.

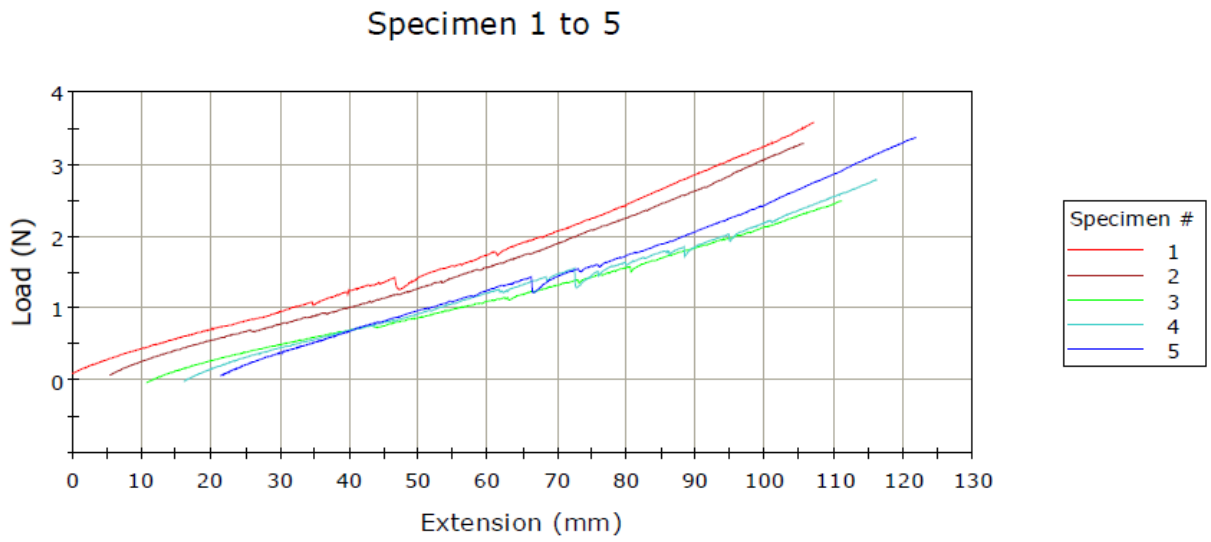

Figure 3.2 Tensile test of five samples of the silicon sheet. The sample dimension used were: 13mm * 100mm * 0.127 mm

3.2.1 Images from the Finite Element Analysis (FEA):

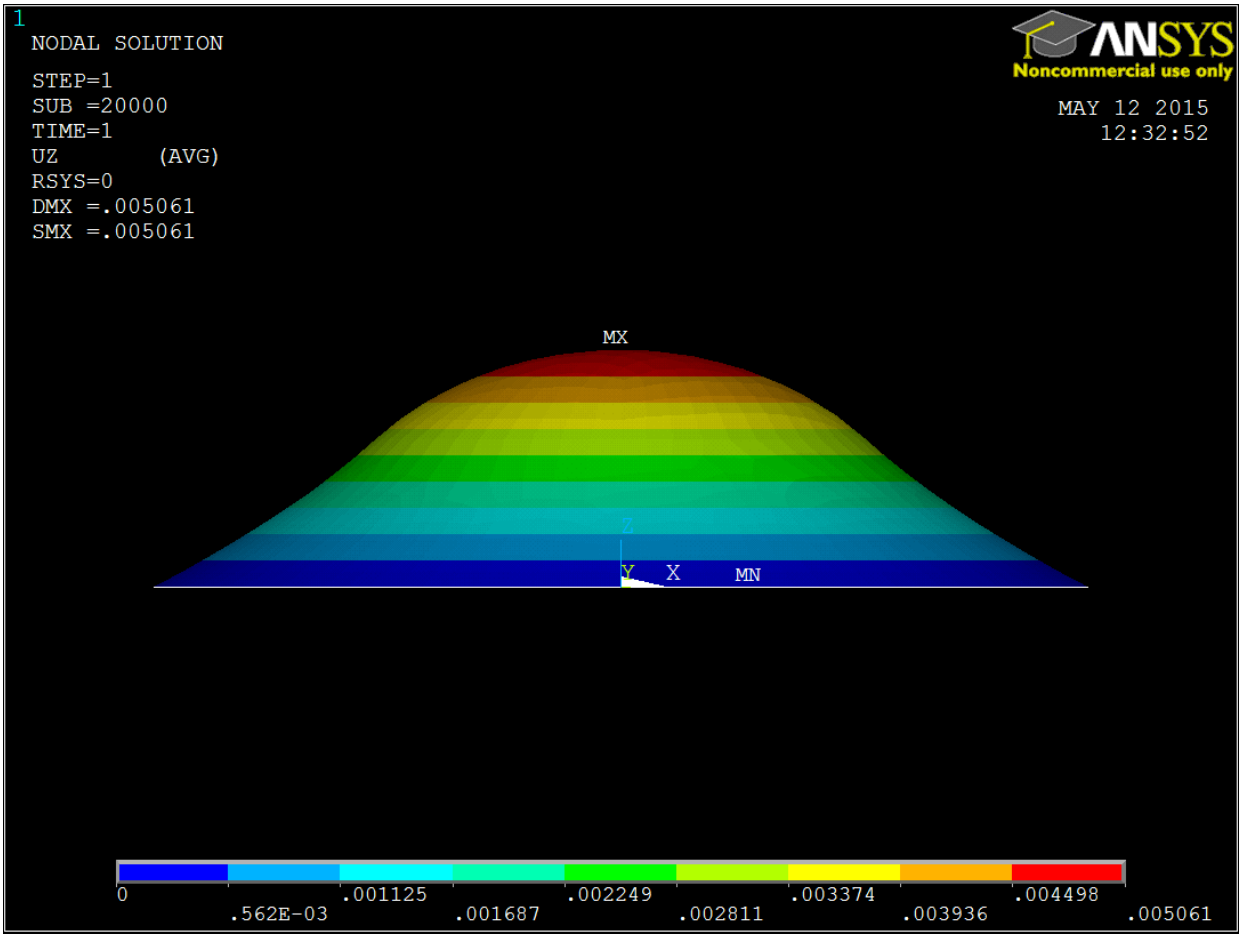

Figure 3.3 Bottom view of the Z-component of displacement. This image represents the real simulation of how the membrane is being deformed during the experiment. It is clearly observable that the membrane deforms in a tent-like shape rather than a bubble-like shape. This is the reason why a different membrane deformation analysis must be used. A FEA is the starting point for this membrane characterization; future work will include an in-depth analysis.

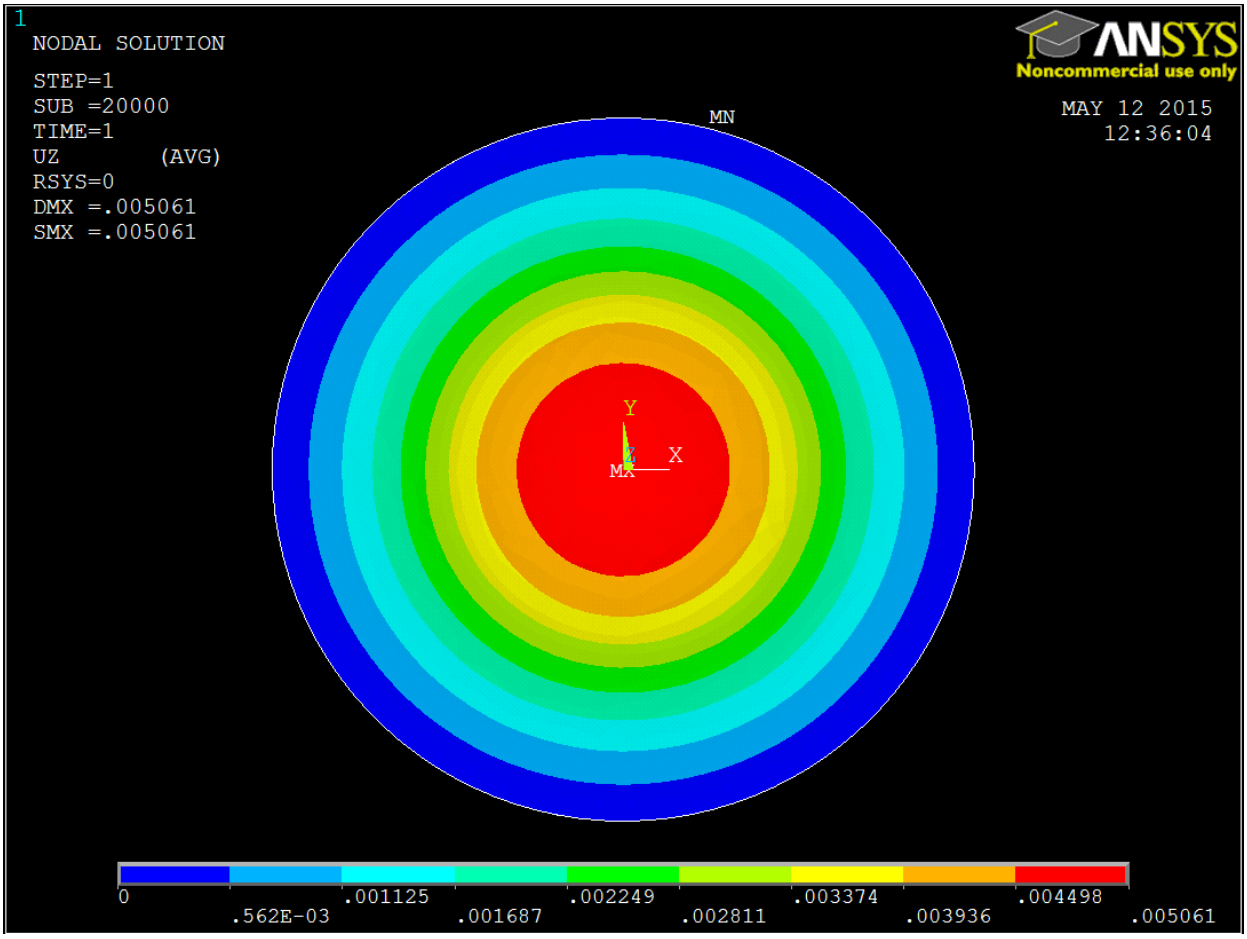

Figure 3.4 Front view of the Z-component of displacement. Based on the colors, one can observe that the edges of the membrane are not moving (blue), whereas, the center of the membrane is displaced by the indenter in the Z-direction (red).

The FEA shows the total mechanical strain distribution in the X or radial, Y or circumferential, and Z directions. Figure 3.5 shows the total mechanical strain in the X or radial direction in Cartesian coordinates. The dark blue color has a negative strain value that corresponds to the contraction of the membrane as it stretches. The other colors have a positive strain value that corresponds to the tensile stretching of the membrane. Figure 3.6 shows the total mechanical strain in the Y or circumferential direction in Cartesian coordinates. The same strain distribution as described above is observed, but in the opposite direction. Figure 3.7 represents the changes in the membrane thickness, which is not of interest for this thesis. It is only shown for comparison of results.

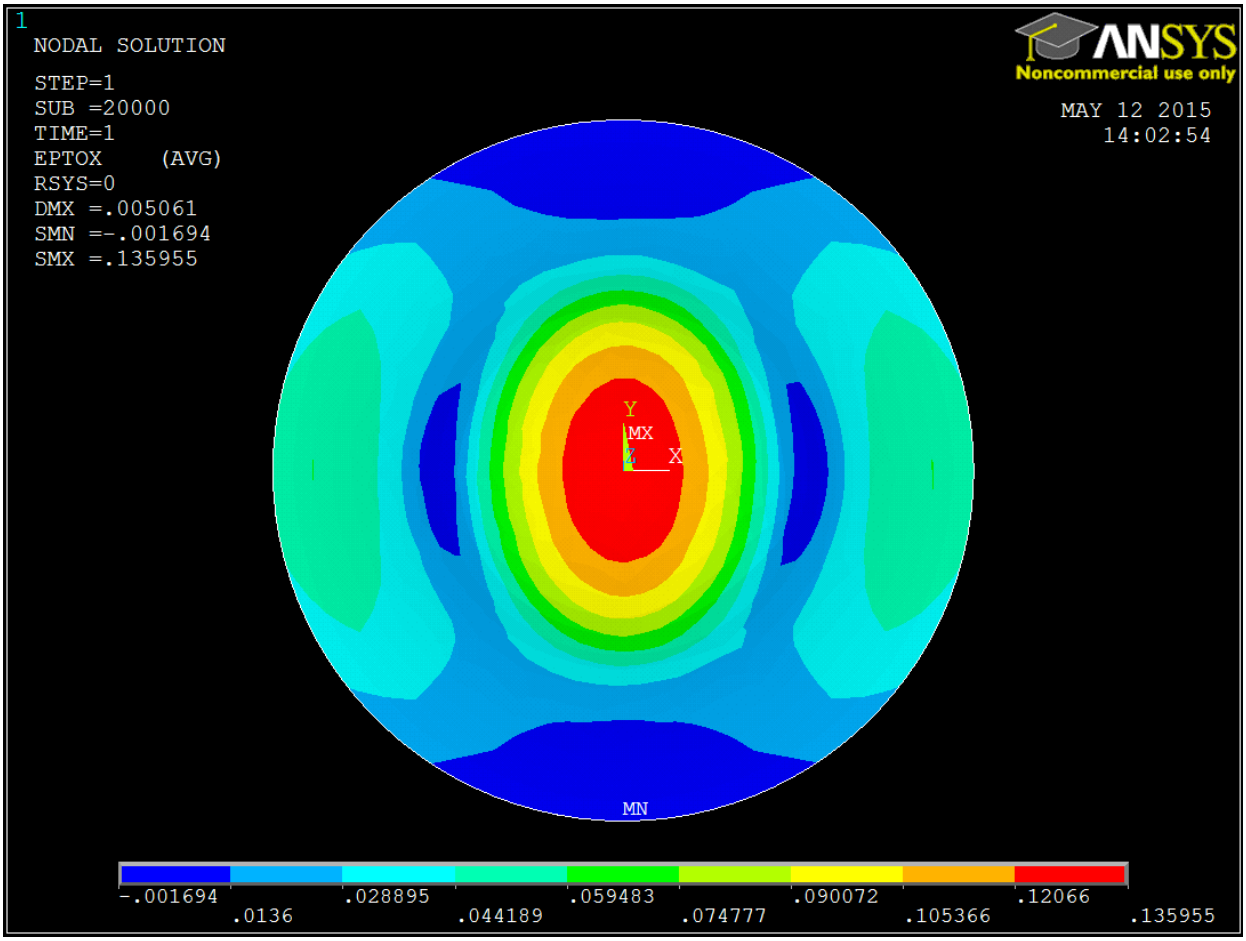

Figure 3.5 X or radial direction of total mechanical strain in Cartesian coordinates.

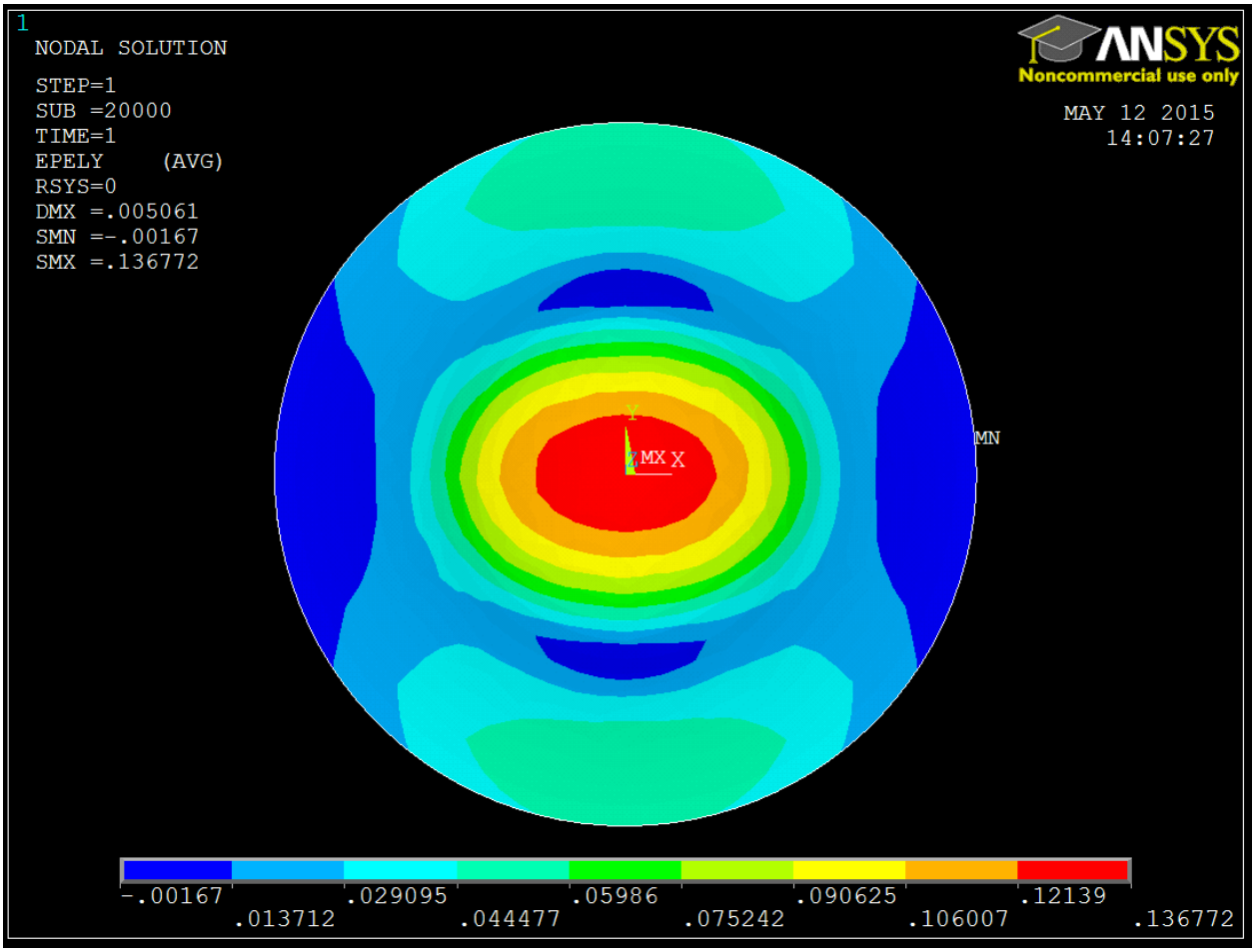

Figure 3.6 Y or circumferential direction of total mechanical strain in Cartesian coordinates.

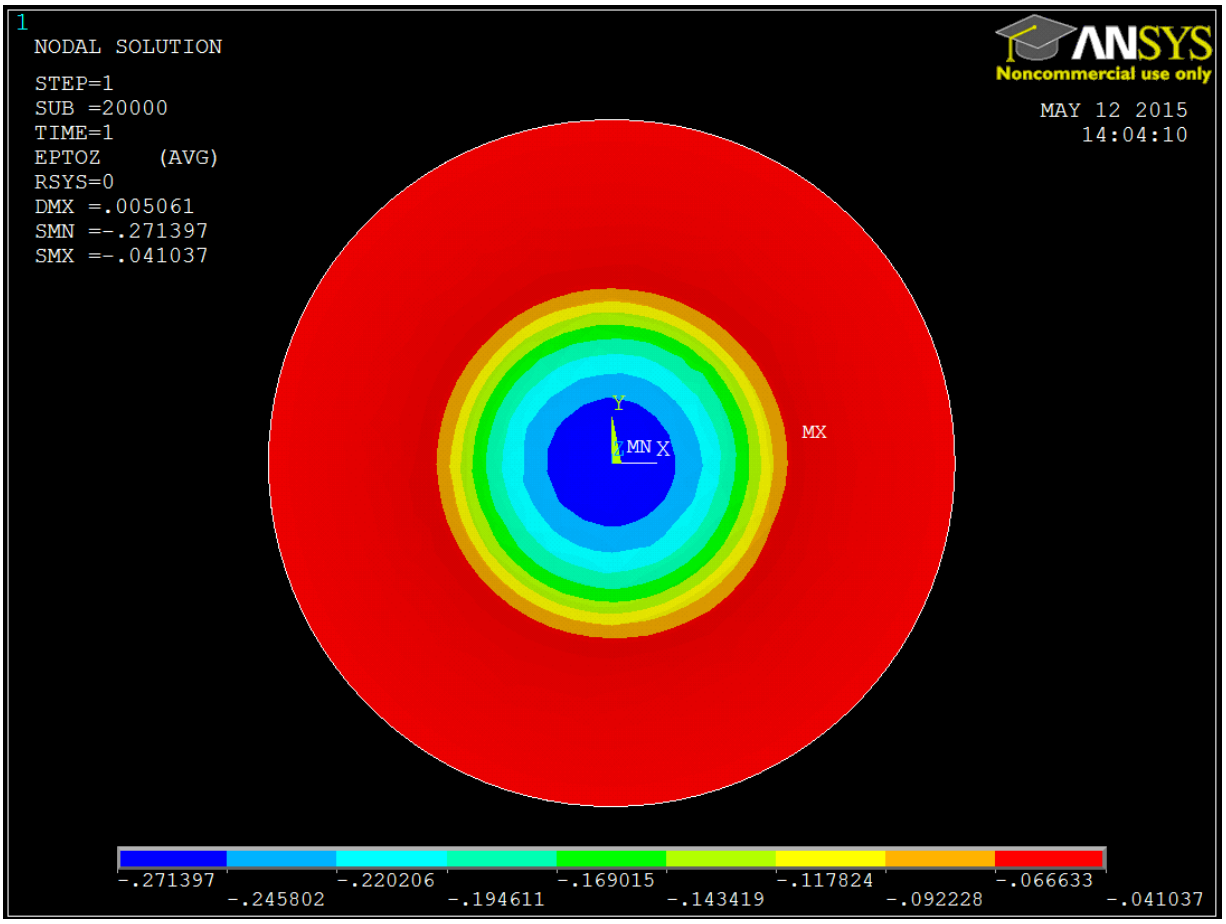

Figure 3.7 Z direction of total mechanical strain in Cartesian coordinates.

There are three principal total mechanical strains which occur along the deformed membrane. The first principal total mechanical strain (Figure 3.8) occurs in the X or radial direction. The membrane undergoes stretching in the radial direction, which is confirmed by the positive strain values. The second principal total mechanical strain (Figure 3.9) occurs in the Y or circumferential direction. As the membrane is stretched, it contracts in the circumferential direction near the clamped area. This is confirmed by the negative strain values of the dark blue area. The third principal total mechanical strain (Figure 3.10) happens in the Z-direction or out of the plane. It defines the change in thickness as the membrane deforms.

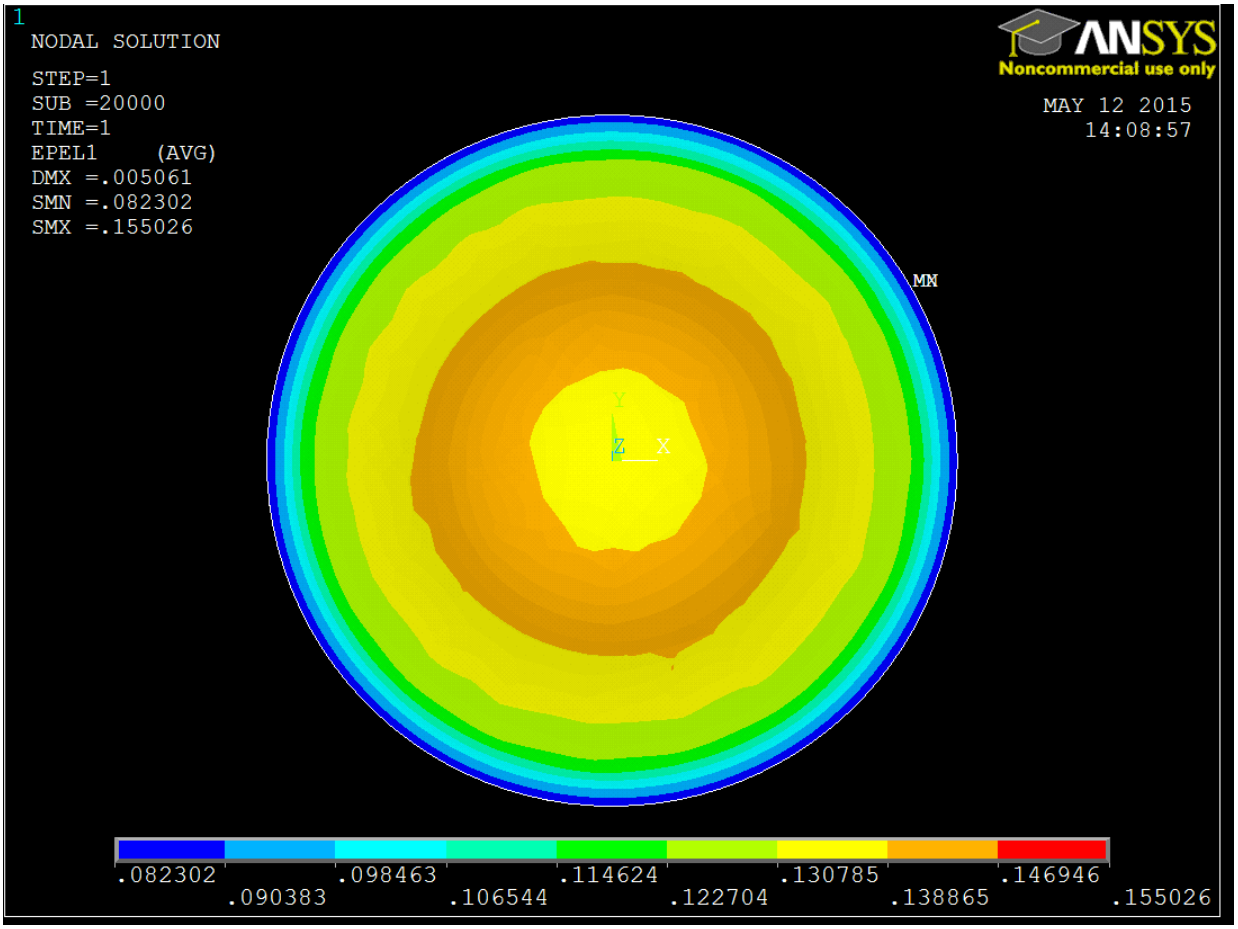

Figure 3.8 1st principal total mechanical strain.

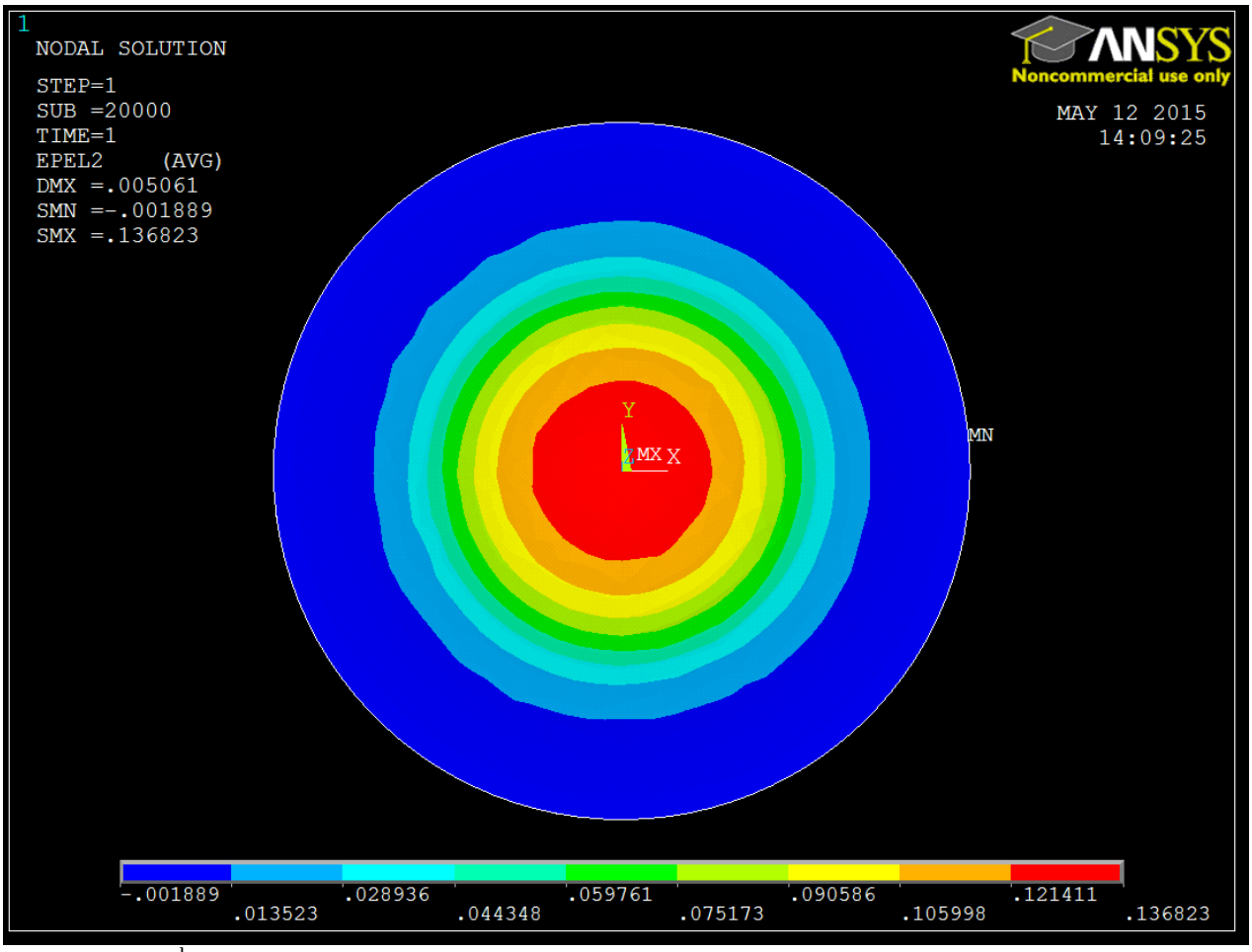

Figure 3.9 2nd principal total mechanical strain.

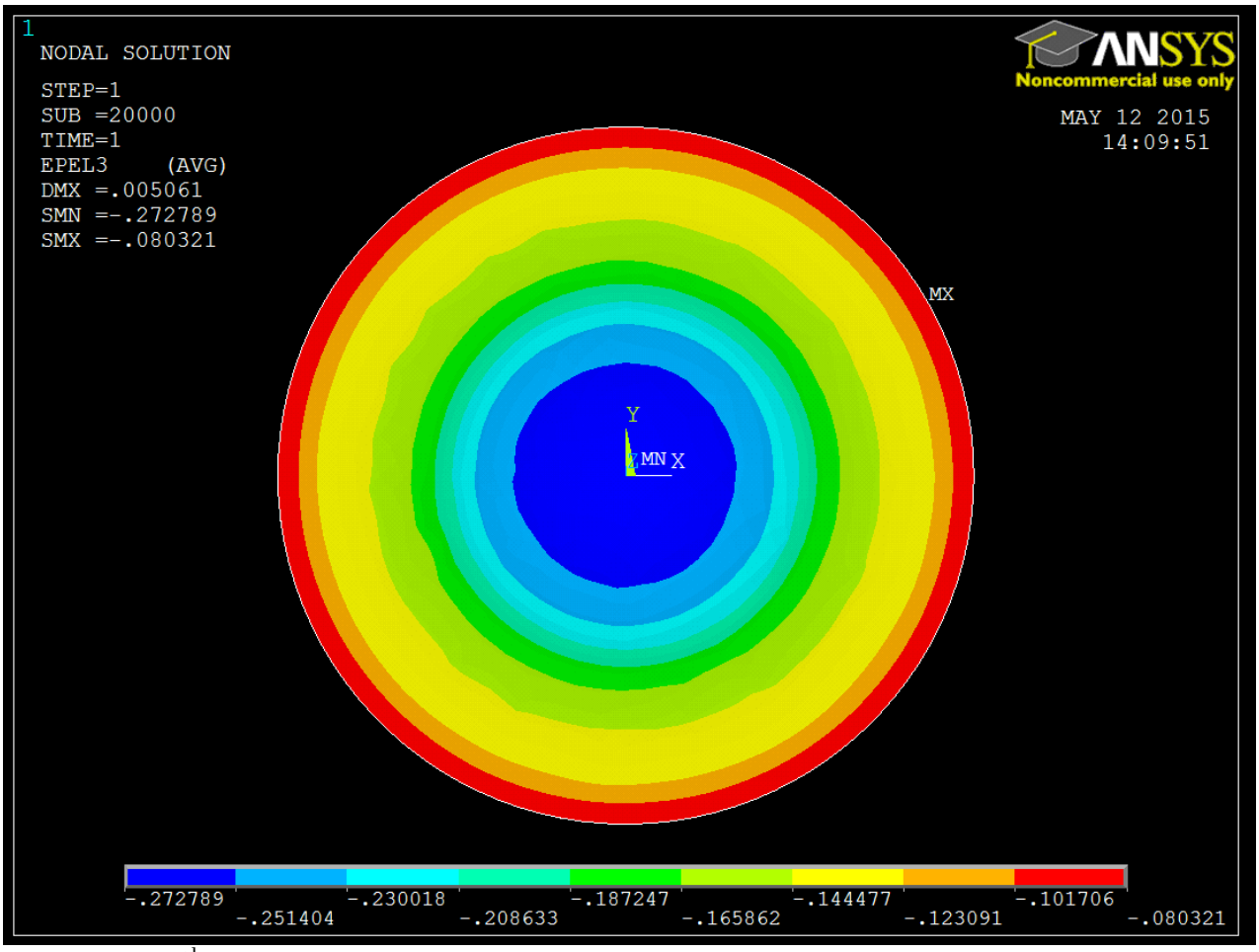

Figure 3.10 3rd Principal total mechanical strain

3.2.2 Parts of the Device

Images 3.5-3.9 show the design characteristics of each part of the device and the assembly of the device:

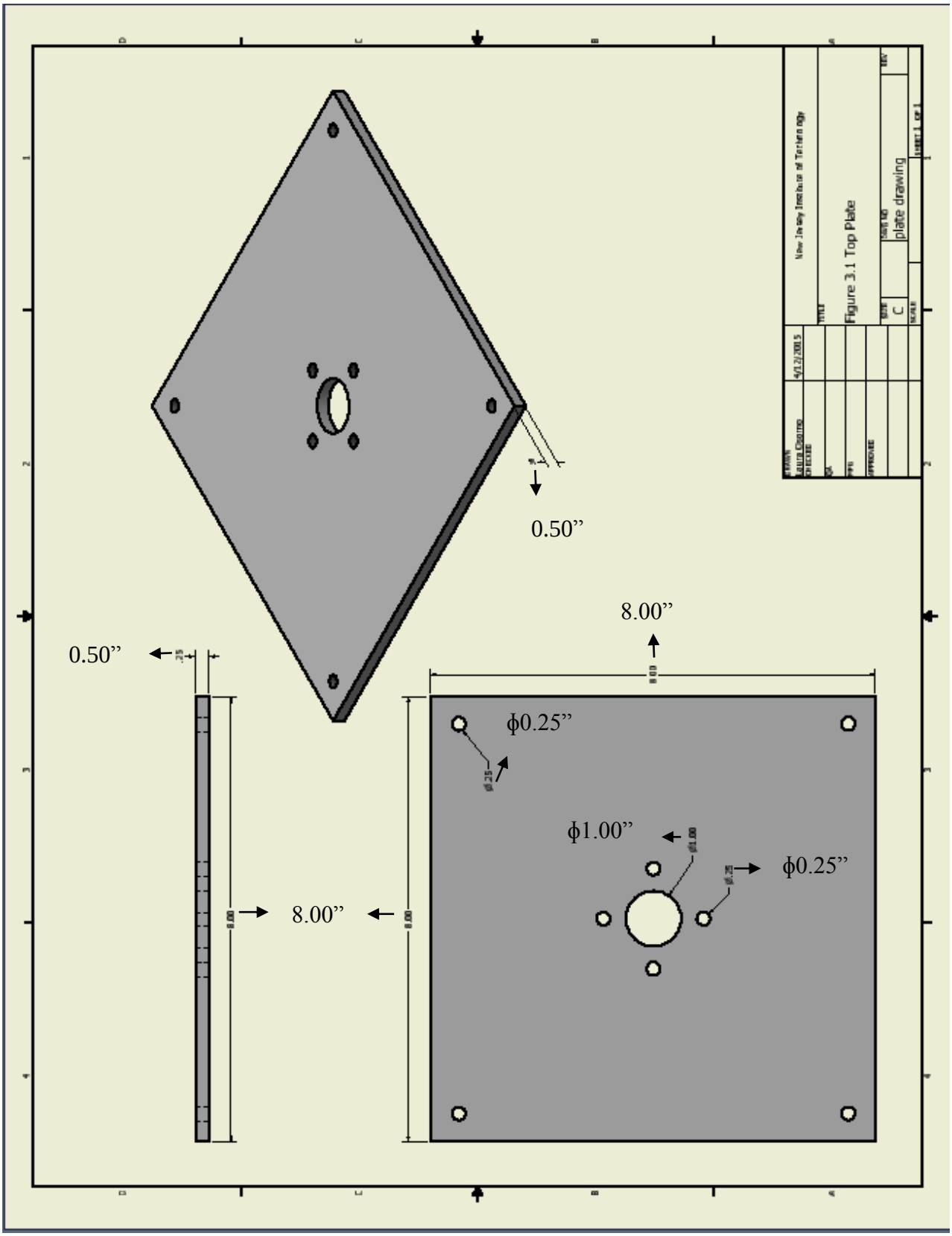

Figure 3.11 Top Plate.

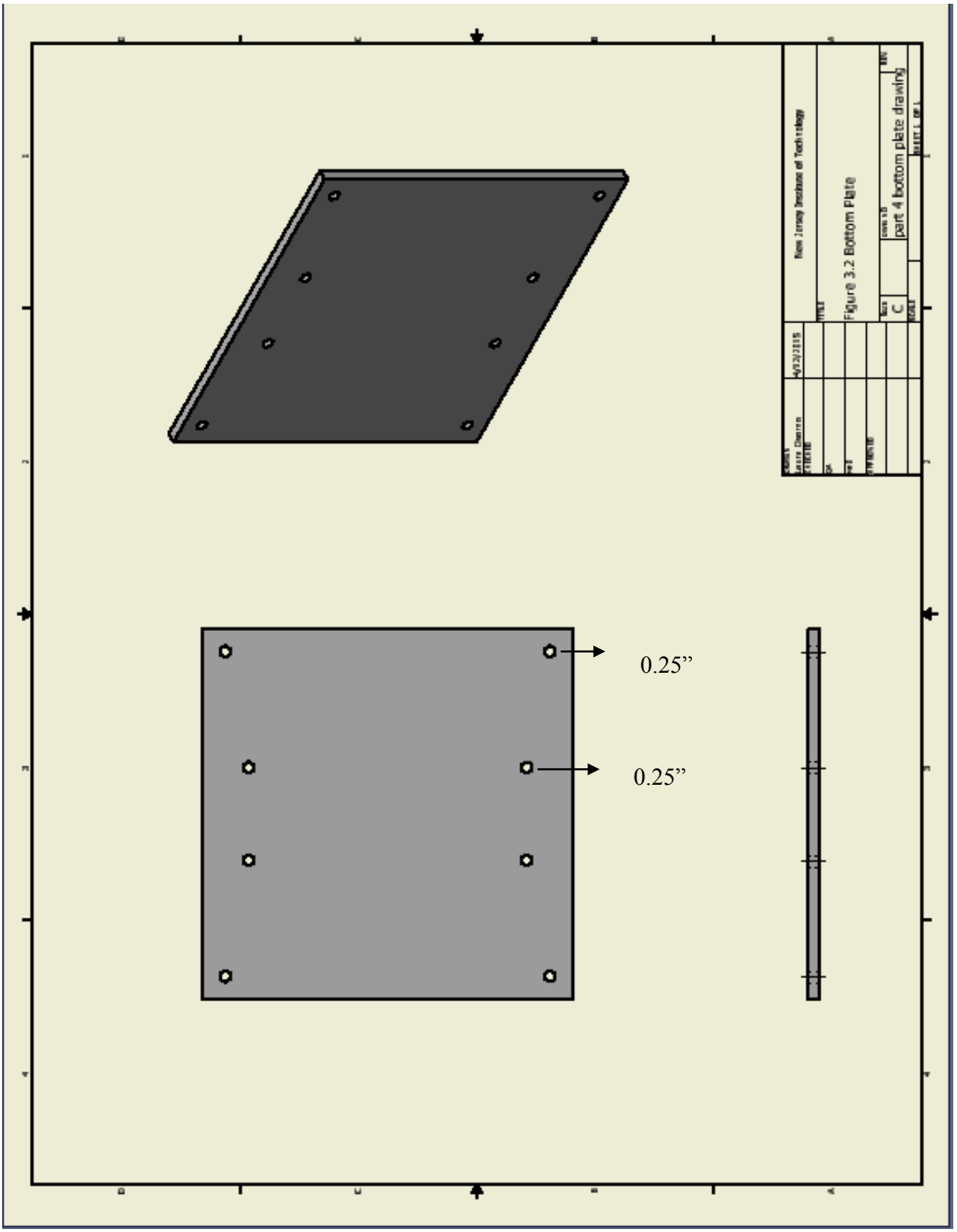

Figure 3.12 Bottom Plate.

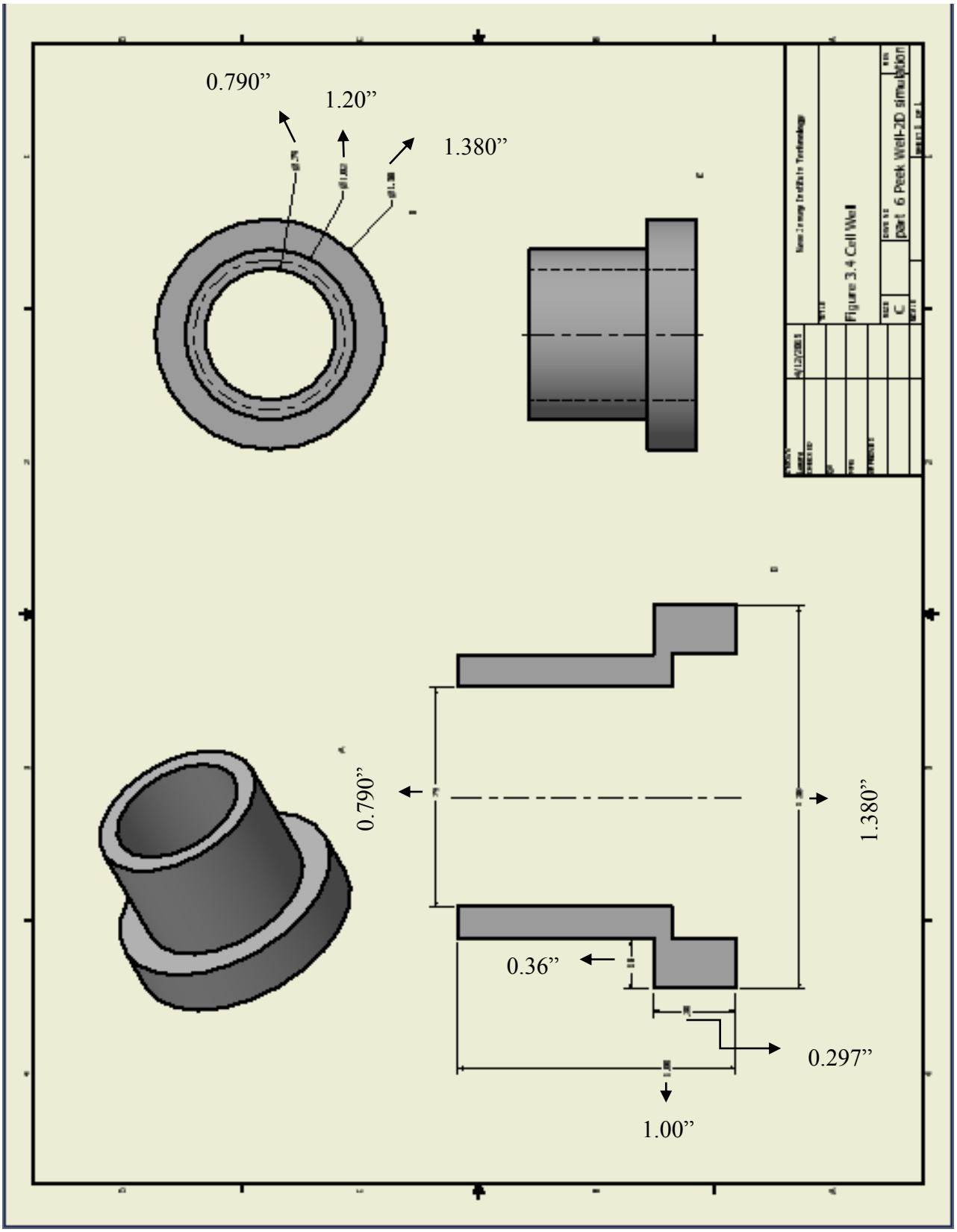

Figure 3.13 Cell Well.

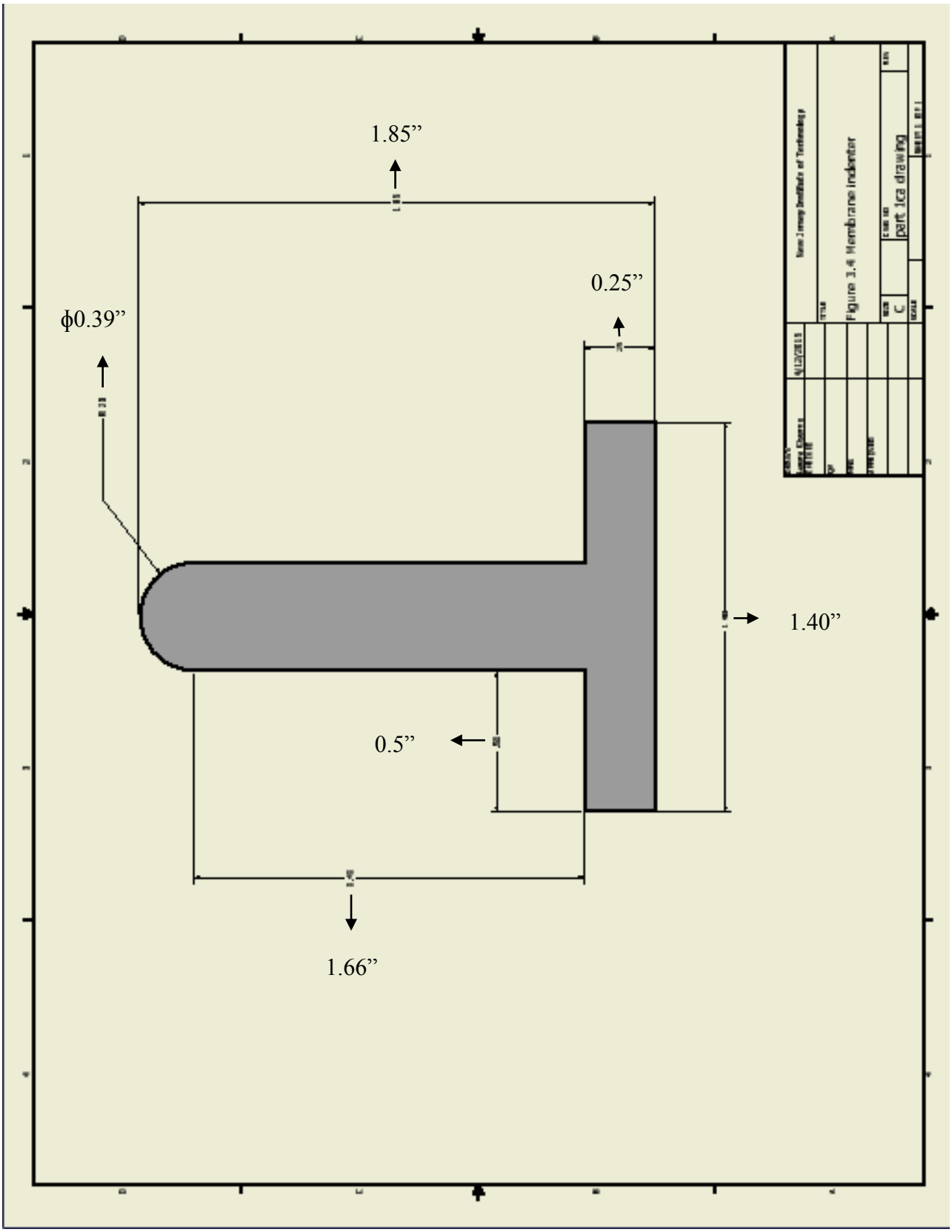

Figure 3.14 Membrane indenter.

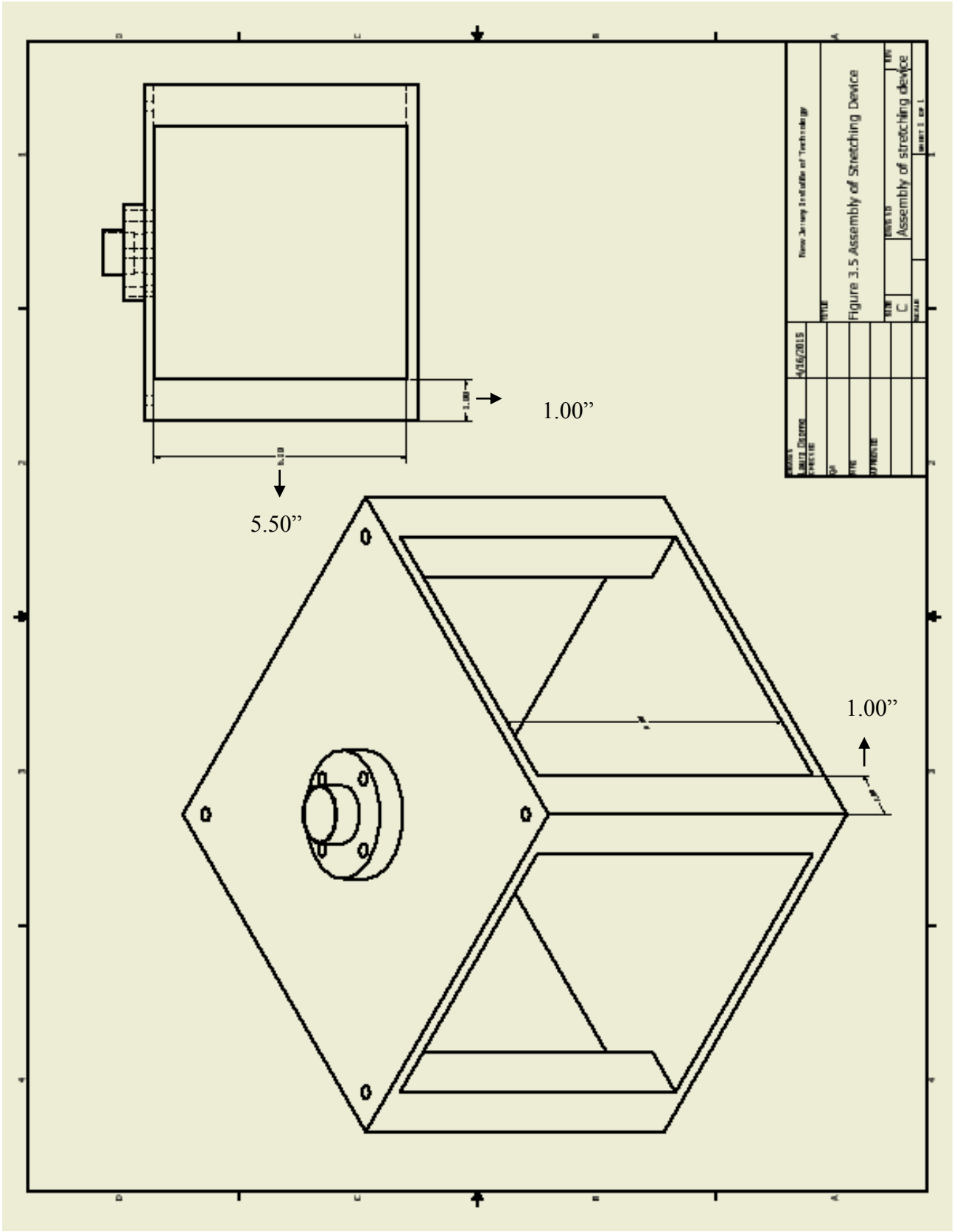

Figure 3.15 Assembly of Stretching Device.

CHAPTER 4

EXPERIMENTS AND PROTOCOLS

4.1 Device Calibration

The device was designed to allow for absolute control of the strain levels. However, it had to be modified to properly measure the vertical displacement to be measured from the top plate, which is the reference point, using a caliper. MATLAB was used in order to solve for the displacement (*a*) from Equation 3.1. The initial placement or the zero point of the membrane measures 37.33 mm from the top plate of the device. In order to obtain 20% strain, the membrane must be displaced 5 mm. Therefore, the caliper must measure 32.5 mm in order to obtain the needed displacement. Table 4.1 shows the different values of vertical displacement with its correspondent strain value.

Table 4.1 Strain values with their corresponding vertical displacements

Strain value (%)	Vertical displacement of the silicon membrane in mm	Number read on the caliper in mm
0	0	37.33
5	20	32.5
10	60	27.5
15	150	22.5
20	420	17.5
21	520	12.5
22	660	7.5
23	830	2.5

After calibration, the strain distribution at 5 mm vertical displacement was checked by drawing circles around the indenter and the clamped area of the membrane. The distances between the inner and outer points were measured respectively before and after the deformation in order to find the approximated strain values using the strain equation:

$$\in = \frac{\Delta l}{l_o} = \frac{l - l_o}{l_0} \qquad 4.1$$

Table 4.2 Experimentally obtained strain values

Strain value at the center of the membrane at 5 mm vertical displacement	**Strain value at the sides of the membrane at 5 mm vertical displacement**
19 ± 0.05 %	0.11 ± 0.03 %

4.2 Cell Culturing

Neonatal human dermal fibroblasts (HDFn) obtained from Dr. Michniak's lab were thawed according to the instructions obtained from Invitrogen (Carlsbad, CA) and plated at a density of 250,000 cells cm^{-2} in T-25 flasks in 5 ml of culture media containing Dulbecco's Modified Eagle Medium (DMEM, Invitrogen) supplemented with 10% fetal bovine serum (FBS, Invitrogen), 1% Penicillin/Streptomycin (P/S, Invitrogen), and 1% L-Glutamine (Invitrogen). The cells were incubated at 37 °C with 5% CO_2 and 95% humidity. Once they reached 90% confluence, the cells were trypsinized using 0.025% Trypsin-EDTA (Invitrogen) until they detached from the bottom of the flask. Then they were counted using Trypan Blue (Sigma). The cells were either re-cultured or seeded onto

a silicon membrane (0.005" Gloss/Gloss silicone sheeting, Specialty Manufacturing, Saginaw, MI) at a density of 11,905 cell cm^{-2} (150,000 cells/ml).

4.3 Preparation and Assembly of the Cell Well

To prepare the cell well for culture, the PEEK rings were washed thoroughly using Sparkleen (Fisher Scientific Co.) laboratory detergent and sonicated three times with purified water. The rings were rinsed with purified water between sonications in order to remove excess waste. The silicon sheeting (0.005" Gloss/Gloss silicon sheeting, Specialty Manufacturing) iss cut into approximately 2 x 2 cm squares. Importantly, the cut silicon sheet had to be washed with RO water. The square pieces of silicon were placed under the large ring and the small ring was press fitted in order to form a stable well. The well was then placed in a plastic container resistant to autoclaving with purified water. The well was autoclaved for one hour.

After autoclaving, the well was allowed to dry and cool to room temperature in a sterile culture hood. The silicon membrane had to be coated using Poly-L-Lysine solution (0.05mg/mL, PLL, Peptides International, Louisville, KY) at a ratio of 5 PLL to 7 of sterile distilled water. The well was left in the incubator at 37 °C overnight. The PLL solution was aspirated. The wells were rinsed three times with sterile distilled water and were allowed to air dry. HDFn were seeded at a density of 150,000 ells/ml. The well with already-seeded cells was left in the incubator at 37 °C for at least 6 to 8 hours.

4.4 Stretching Experiment

Before and after the stretching experiments, the cells were imaged. The center of the silicon well was marked as a reference point for properly imaging the cells. The cell well was then placed on top of the top plate of the stretching device, and the well holder was then placed on top of the cell well, providing better support. The well holder was tight using 12/64” screws (McMaster-Carr). The four small glass flasks had to be filled with DI water, and the glass cover had to be placed on top of the metal box surrounding the cell well. In order to achieve 20% strain at the center of the membrane, the membrane had to be vertically displaced 5 mm. The initial positon of the mechanical jack was at 37.33 mm, which positions the indenter right below the membrane. A 5 mm vertical displacement of the membrane read as 32.5 mm on the caliper (Table 4.1). The cells were left under static point load deformation for one hour.

4.5 Cell Viability Quantification

After one hour deformation, the regular procedure for passing and counting cells was used. Cells were trypsinized with 0.025% Trypsin-EDTA (Invitrogen); two micro-centrifuge tubes with cell suspension were prepared as samples to count the cells. From each sample, the cells were counted three times using Trypan Blue (Sigma) and a Hemocytometer, making a total of 6 counts. This allowed for statistical analysis. Both the live and dead (stained in blue) cells were counted separately. Equation 4.1 is the cell viability equation used to find the cell viability percentage.

$$\begin{aligned} Cell\ Viability\ (\%) & \\ &= total\ viable\ cells\ (unstained) \\ &\div total\ cells\ (stained\ and\ unstained) * 100 \end{aligned} \tag{4.2}$$

CHAPTER 5

RESULTS

The main purposes of these experiments were to: 1) prove whether or not the device is sufficient to model rapid stretching of the skin, as observed in pregnancy, weight gain, and tissue expansion, leading to stretch marks formation; 2) to analyze cell morphology, change in cell polarity, and cell viability as a function of total strain, and 3) to understand the basic development of stretch marks.

A total of two experiments were conducted for one hour at 20% strain. Cell images were taken before and after the deformation period, and they were also counted in order to calculate cell viability. Images 5.1- 5.4 represent the results from experiments 1, and 2.

5.1 Experiment 1

Pre-stretched cells:

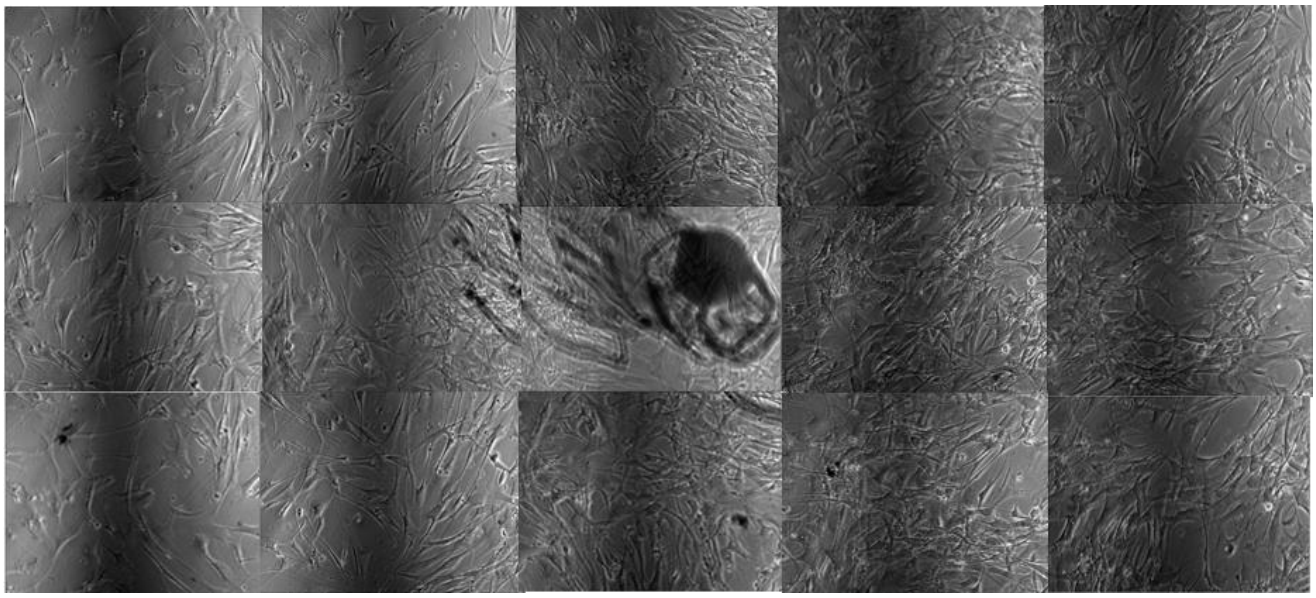

Figure 5.1 HDFn before deformation at a magnitude of 10X.

One hour after deformation at 20% strain:

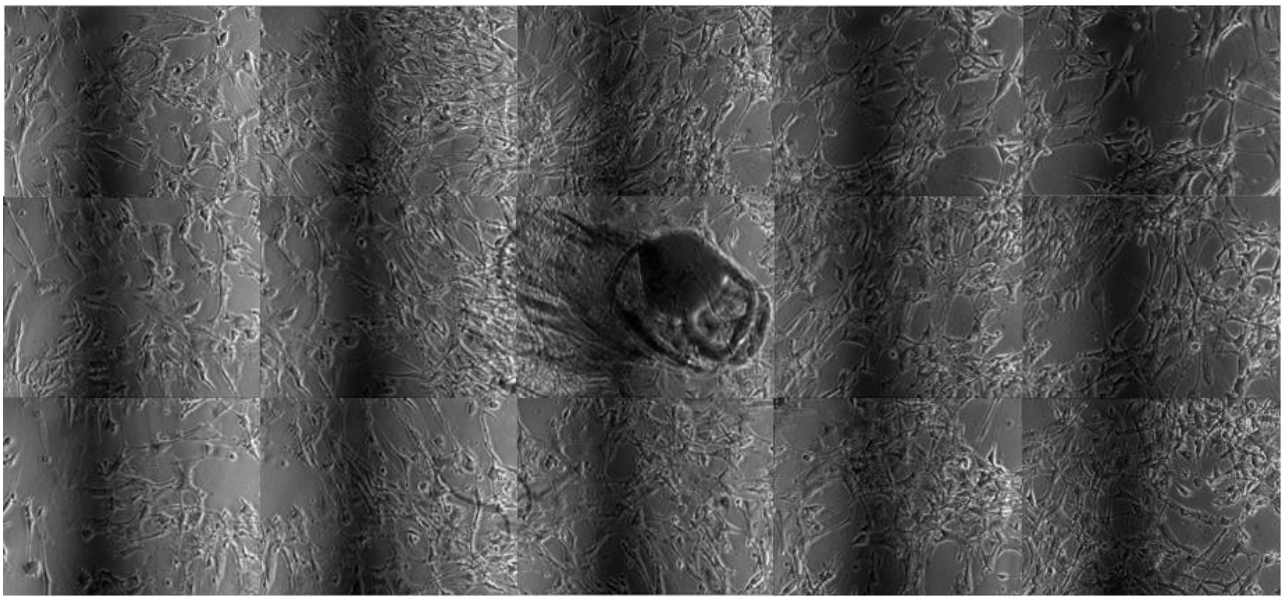

Figure 5.2 HDFn one hour after deformation at 20% strain at a magnitude of 10X.

Cell Quantification:

Table 5.1 Cell quantification of experiment 1

Live	**Dead**
100,000 ± 22,000	140,000 ± 60,000

Cell Viability:

After applying the formula 4.2, 42 % of the cells in the culture were alive after deformation.

5.2 Experiment 2

Pre-stretched cells:

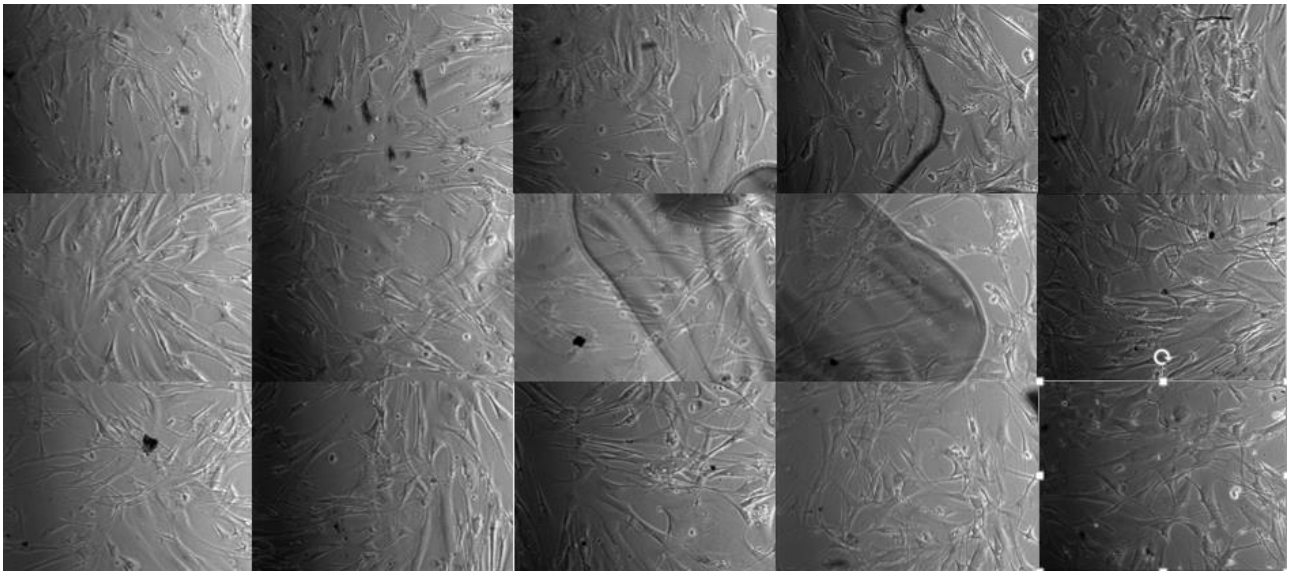

Figure 5.3 HDFn before deformation at a magnitude of 10X.

One hour after deformation at 20% strain

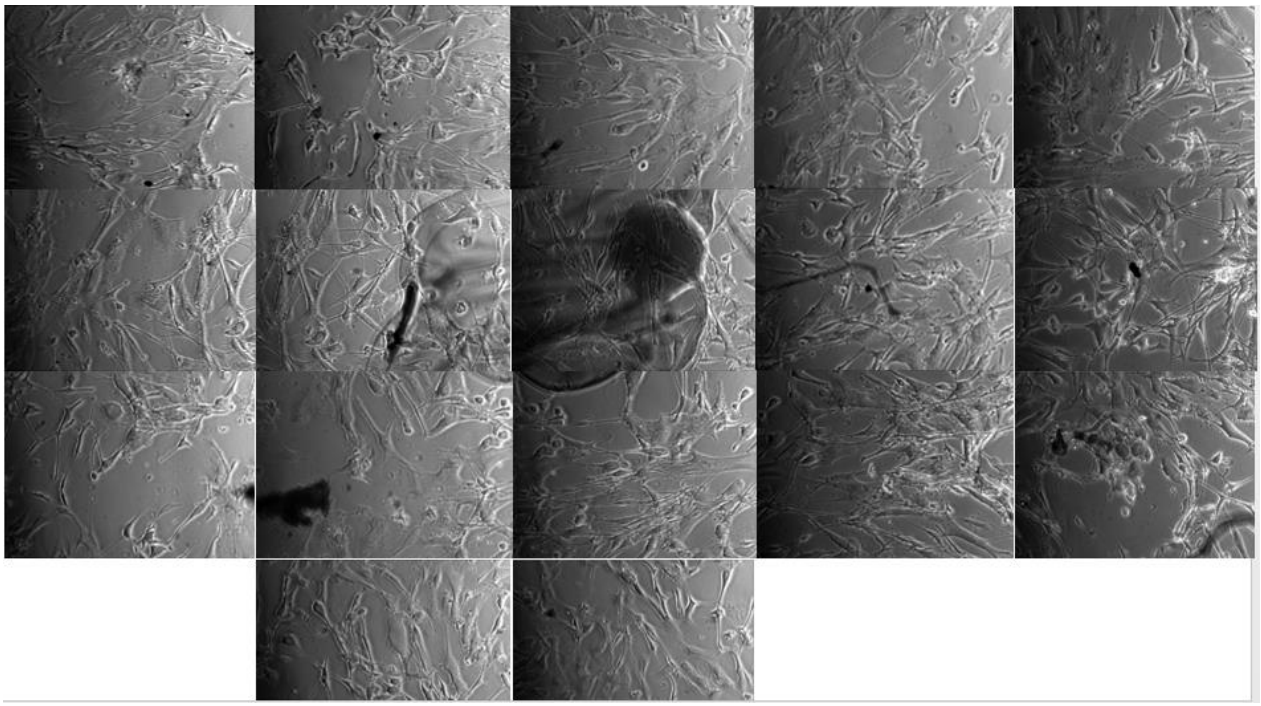

Figure 5.4 HDFn one hour after deformation at 20% strain at a magnitude of 10X.

Cell Quantification:

Table 5.2 Cell quantification of experiment 2

Live	Dead
60,000 ± 40,000	100,000 ± 20,000

Cell Viability:

After applying the formula 4.2, 38 % of the cells in the culture were alive after deformation.

5.3 Morphological Changes

Cells present morphological differences before and after deformation. Before deformation, the HDFn are elongated, with well distinguished nucleus and clear branched out cytoplasm. After deformation, the cells are acquiring a rounded structure as if they were starting to detach from the membrane. The comparison of two images (before and after stretch) of experiment 1, 2, and 3 respectively, allows one to observe a drastic change in the morphology of the cells.

5.3.1 Comparison between Cells before and after Deformation from Experiments 1 and 2

Images 5.5 and 5.6, from the same area towards the left side edge of the membrane, before and after deformation respectively from experiment 1, are compared in order to analyze the morphological changes of the cells as a function of strain.

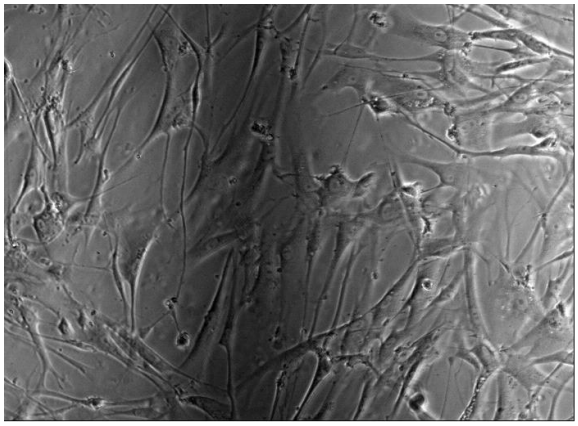

Figure 5.5 Pre-stretched cells, experiment 1 at 10X.

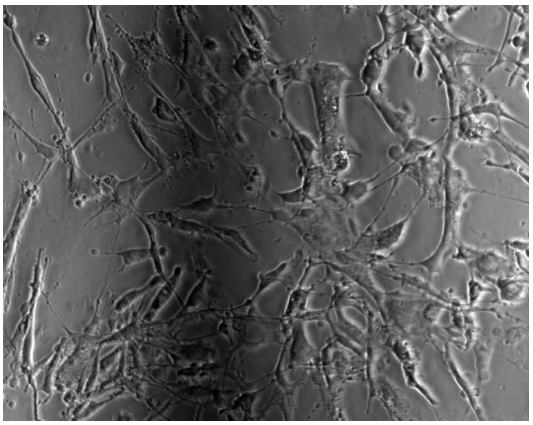

Figure 5.6 One hour after deformation 20% strain, experiment 1 at a magnitude of 10X.

Figures 5.7 and 5.8 also show a morphological change. Before deformation, the cells (Figure 5.7) are flat and elongated with branched cytoplasm whereas, after deformation (Figure 5.8), the cells have acquired a thick rounded shape, which usually happens when they are threatened, in this case by mechanical forces.

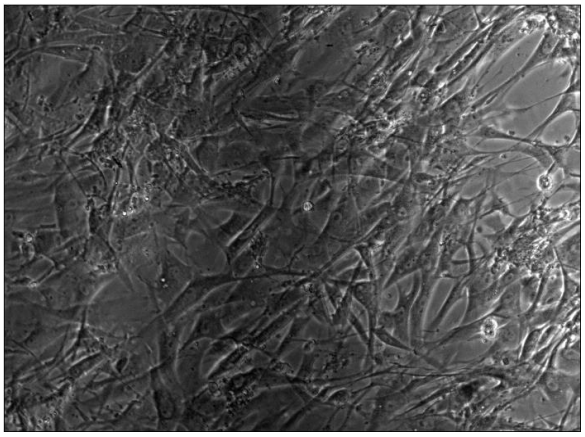

Figure 5.7 Pre-Stretched cells at the center from experiment 1 at 10 X.

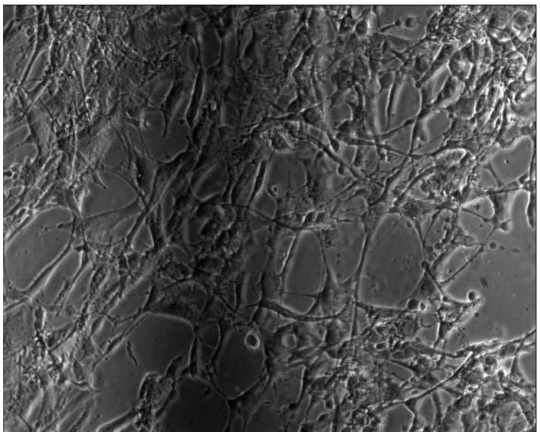

Figure 5.8 One hour after deformation at 20% strain from experiment 1 at a from experiment 1 at 10X.

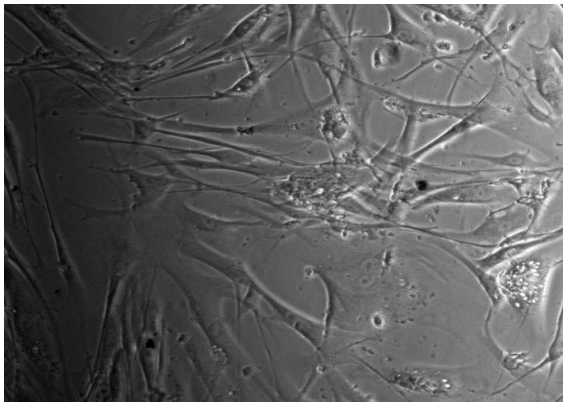

Figure 5.9 Pre-Stretched cells at the center from experiment 2 at 10X.

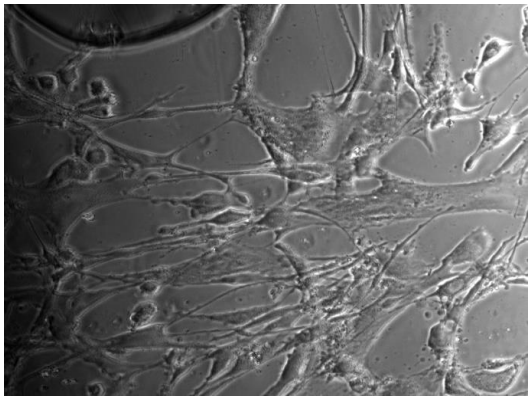

Figure 5.10 Center of the membrane one hour after deformation at a 20% strain from experiment 2 at a 10X.

At the center of the membrane, cells after deformation (Figures 5.8 and 5.10) tend to form small groups, compared to the cells before stretch which are well dispersed on the silicon membrane. As previously mentioned, after stretching, the cells become rounded, and there are more visible spaces on the membrane, as if they were dying. This fact is supported by cell quantification from experiment 1 and 2, which shows that around 140,000 ± 60,000 and 100,000 ± 20,000 cells/ml are dying respectively, because of either excessive or prolonged forces applied to the membrane. This is further confirmed by the cell viability quantification, demonstrating that the majority of the cells from both cultures are dead. This is concluded because the viability percentage is less than 50% (Chapter 5, Sections 5.2 and 5.3).

5.4 Cell Migration

It is clearly visible that cells are moving. To quantify cell movement measurements of the angles of three cells before and after deformation from experiment 1 were taken. However, because of the high cell density, it is very difficult to select the exact cells without a proper marker to identify them. Images 5.13 – 5.15 are polar plots of the measured angles from the three selected cells. They are only shown to demonstrate the

technique used for measuring cell mobility, even though it is not the ideal technique to be for the data analysis of this thesis.

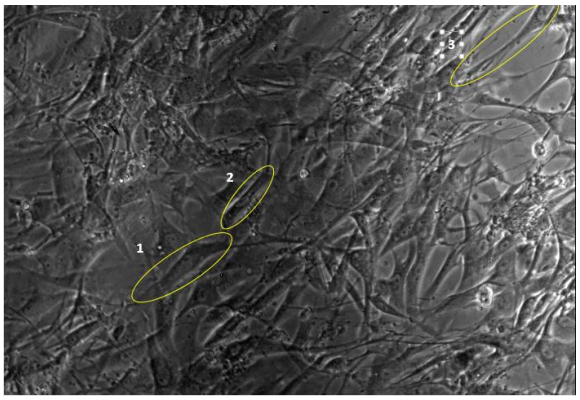

Figure 5.11 Selection of three pre-stretched cells from experiment 1 at 10X.

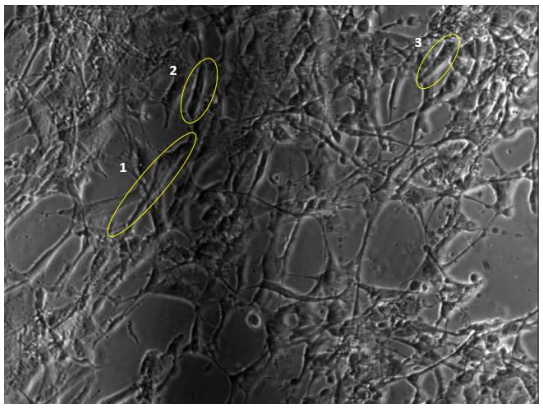

Figure 5.12 Selection of the same three cells from experiment 1 after one hour of deformation at 20% strain 10X.

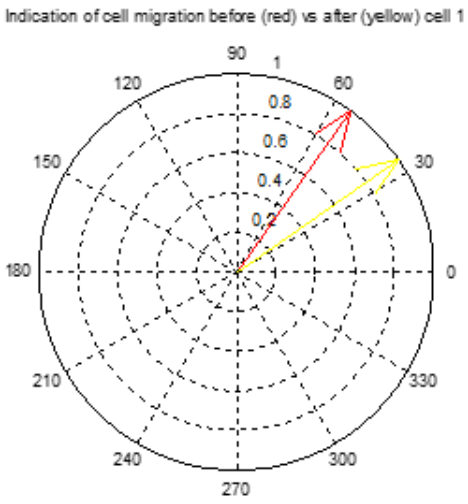

1) Pre-stretched angle: 24.5°
Post-stretched angle: 38.8°

Figure 5.13

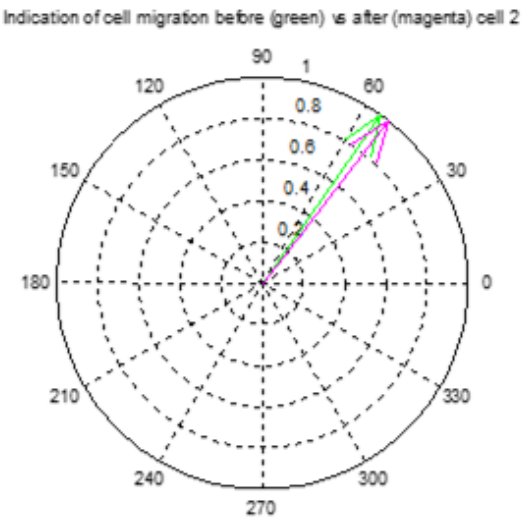

2) Pre-stretched angle: 54.6°
Post-stretched angle: 52°

Figure 5.14

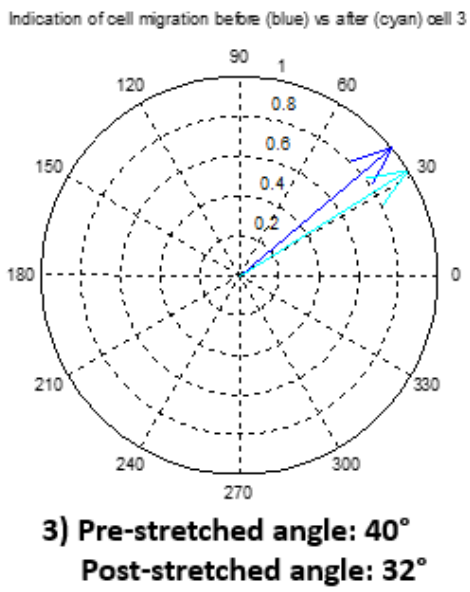

Figure 5.15

5.5 Cell Polarity

As a means of demonstrating that cells change polarity after deformation, lines were drawn on elongated polar cells with branched cytoplasm and a well formed nucleus, from randomly selected images of the membrane before and after deformation from both experiments. The lines were then counted to statistically quantify cell polarity before and after stretch. From experiment 1, three images were easily picked out from the same section of the membrane. However from experiment 2, this technique was applied to analyze the changes of cells as a population. Figures 5.22 and 5.25 are bar graphs representing the amount of elongated-polar cells before and after deformation respectively. These graphs become supportive evidence of the fact that cells experience a severe morphological change while being exposed to mechanical forces.

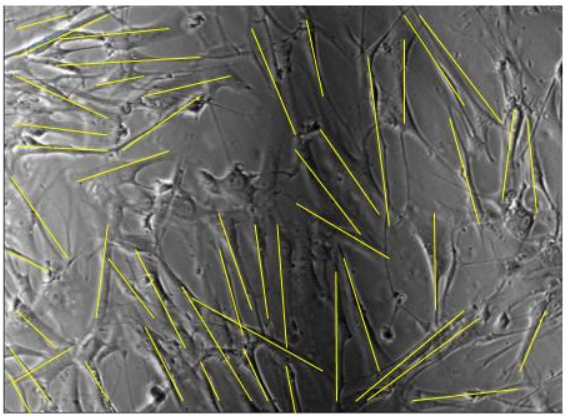

Figure 5.16 Sample 1 quantification of cell polarity from experiment 1 at 10X. Lines were drawn through the elongated-polar cells.

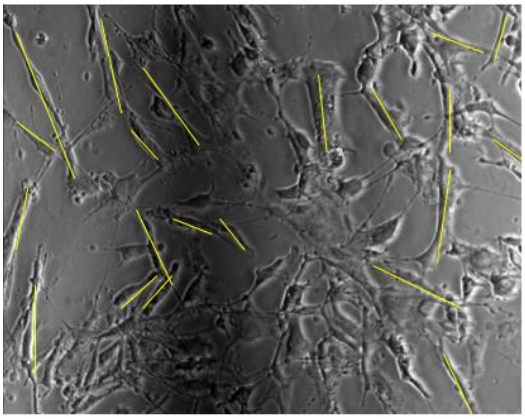

Figure 5.17 Sample 1 quantification of cell polarity after one hour deformation at 20% strain from experiment 1 at 10X. Lines were drawn through the remaining elongated cells.

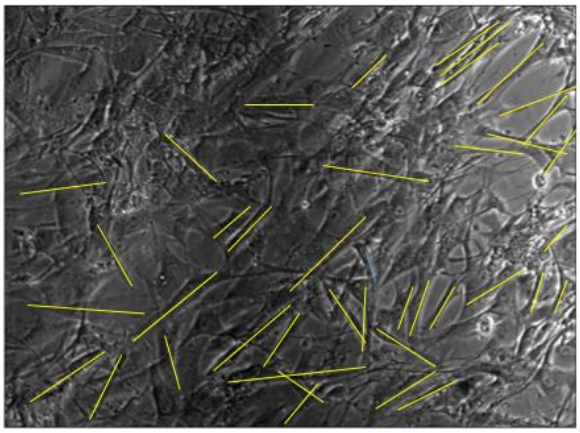

Figure 5.18 Sample 2 quantification of cell polarity from experiment 1 at 10X. Lines were drawn through the elongated-polar cells.

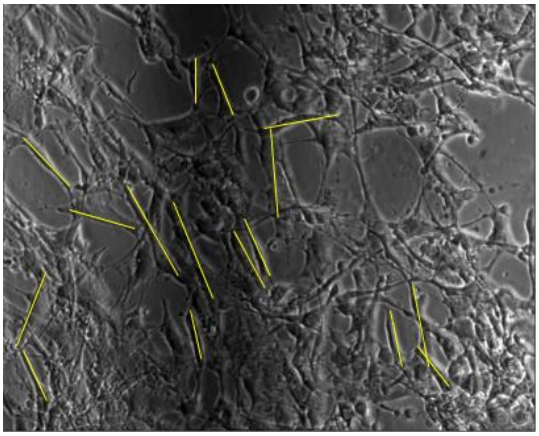

Figure 5.19 Sample 2 quantification of cell polarity after one hour deformation at 20% strain from experiment 1 at 10X. Lines were drawn through the remaining elongated cells.

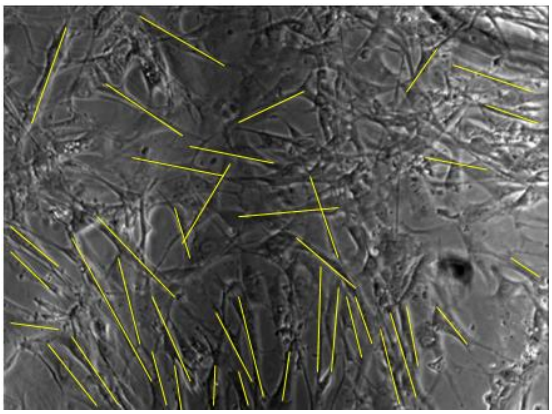

Figure 5.20 Sample 3 quantification of cell polarity from experiment 1 at 10X. Lines were drawn through the elongated-polar cells.

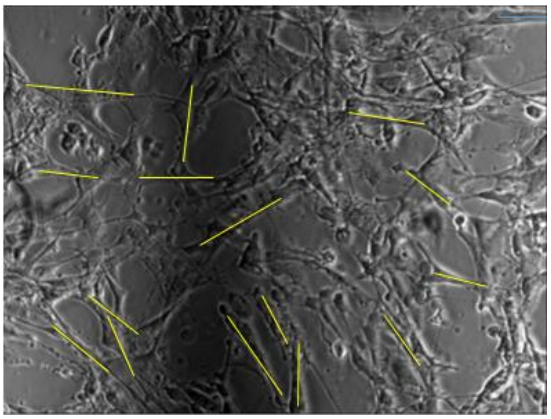

Figure 5.21 Sample 3 quantification of cell polarity after one hour deformation at 20% strain from experiment 1at 10X. Lines were drawn through the remaining elongated cells.

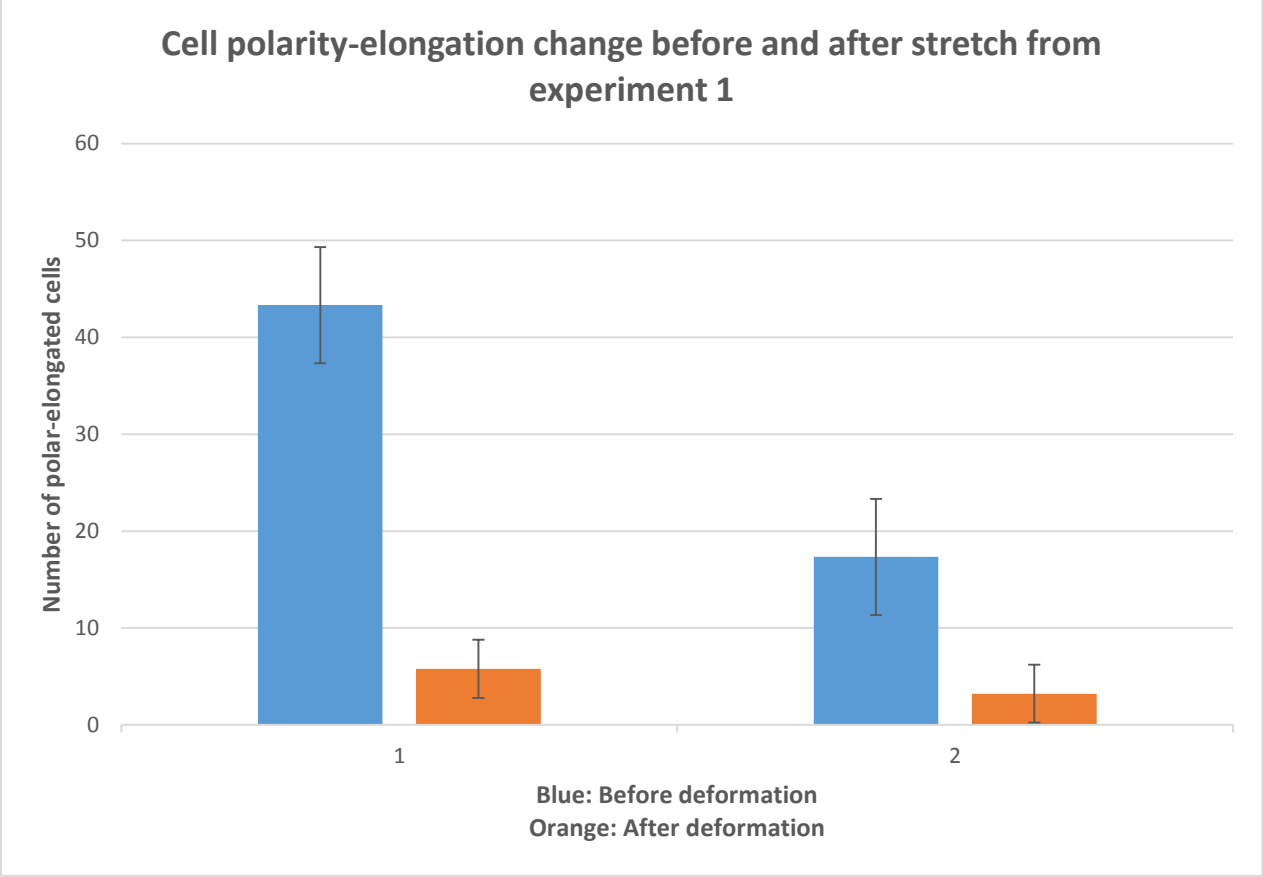

Figure 5.22 Bar graph of cell polarity before and after stretch from samples of experiment 1. After stretch, there are very few elongated and healthy cells, because the cell morphology changes based on the applied mechanical forces. There is an average of 43 ± 6 elongated – polar cells before the membrane is deformed. After membrane deformation, there is an average of 17 ± 3 elongated – polar cells

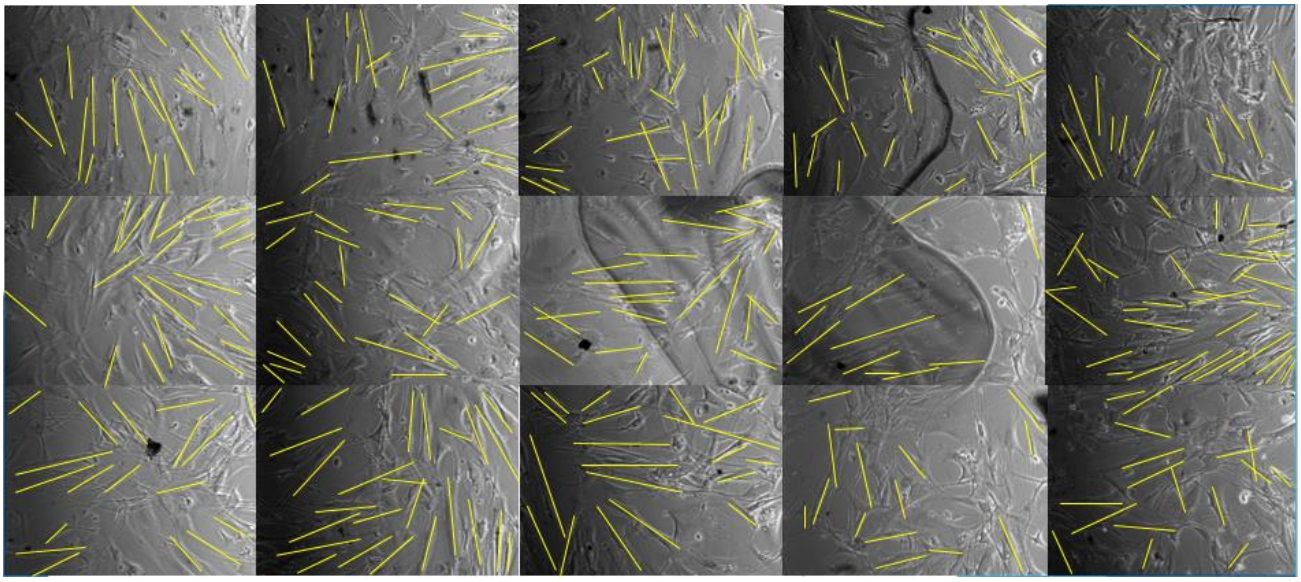

Figure 5.23 Quantification of cell polarity across the silicon membrane before stretch, from experiment 2 at 10X. Lines were drawn on elongated-polar cells with expanded cytoplasm and a clear identifiable nucleus. There is an average of 303 elongated-polar cells after stretch.

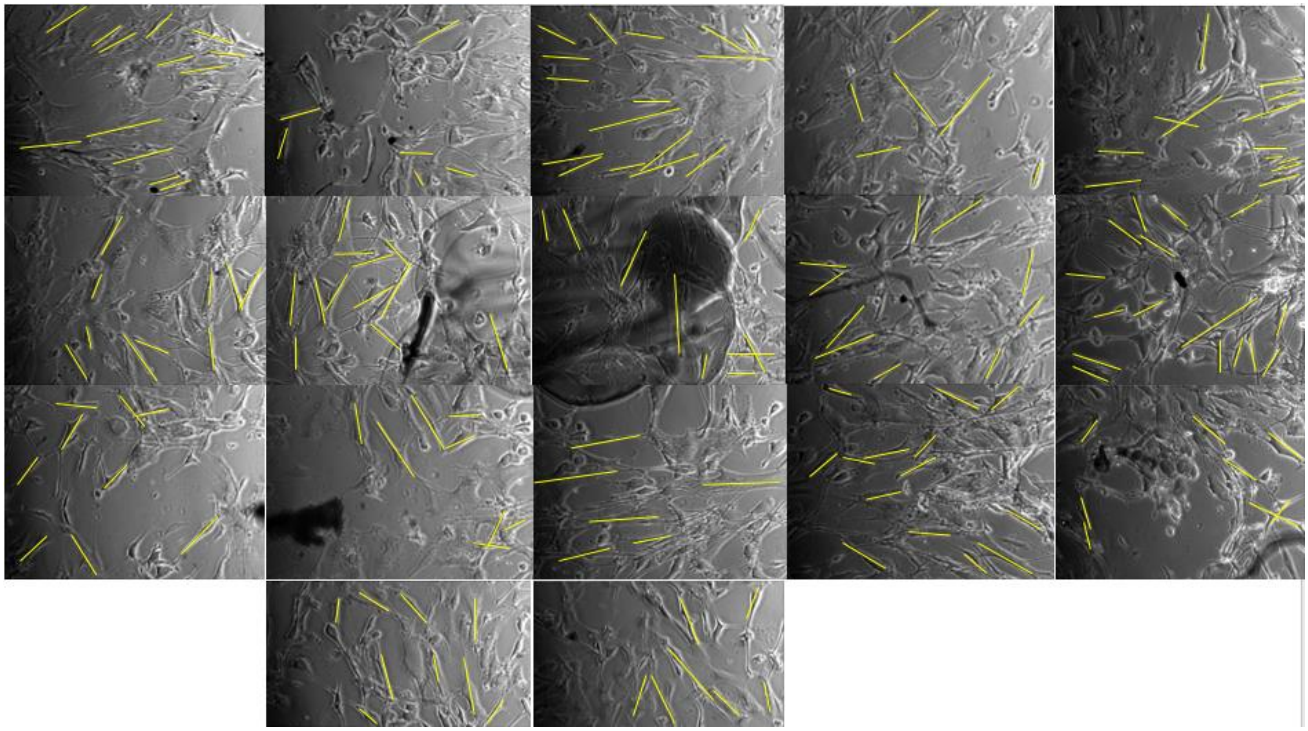

Figure 5.24 Quantification of cell polarity across the silicon membrane after stretch, from experiment 2 at 10X. Lines were drawn on elongated-polar cells with expanded cytoplasm and a clear identifiable nucleus. There is an average of 170 remaining elongated-polar cells after stretch. At a magnitude of 10X.

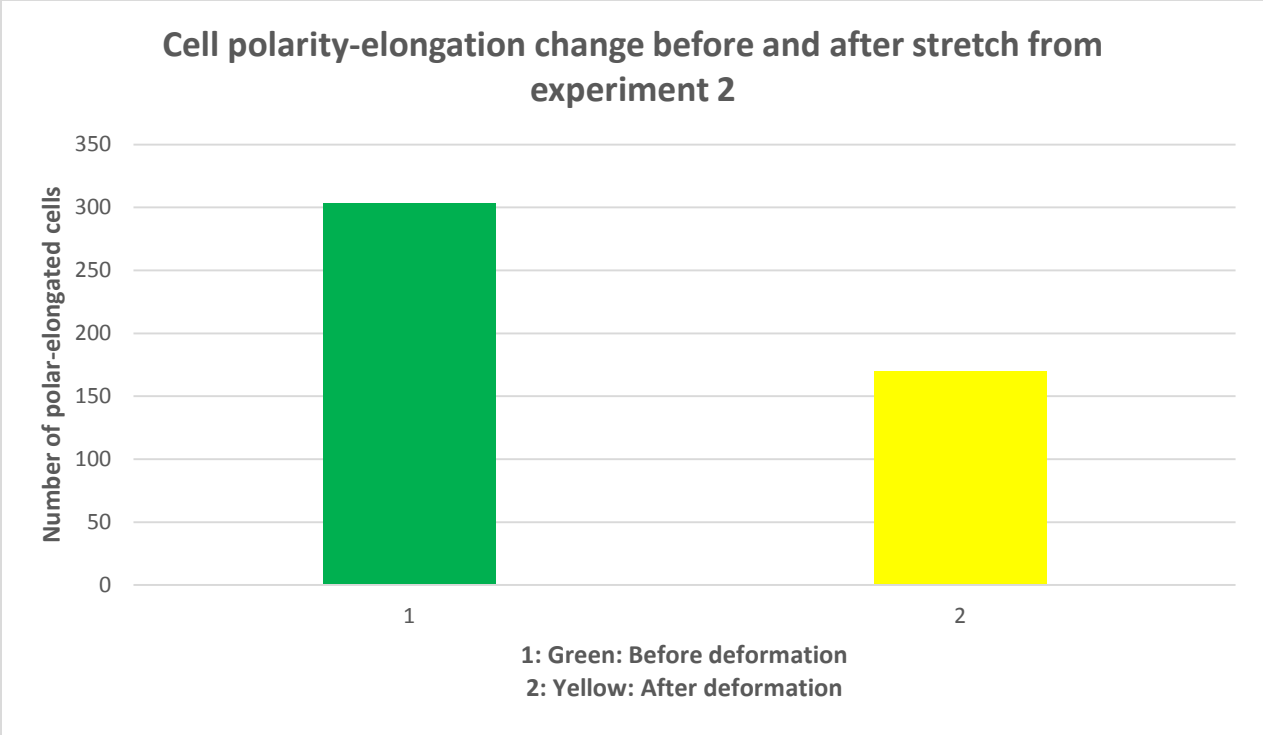

Figure 5.25 Bar graph of cell polarity before and after stretch of experiment 2. After stretch, there are very few elongated and healthy cells because the cell morphology changes based on the applied mechanical forces. There is an average of 303 elongated – polar cells before the membrane is deformed. After membrane deformation, there is an average of 170 elongated – polar cells.

CHAPTER 6

DISCUSSION

The main purpose of this thesis is to use the designed multi-axial stretching device as a model to mimic skin stretched by a normal force as observed during pregnancy, weight gain, body building, and the use of tissue expanders for reconstructive treatments. The designed stretching device allows a maximum strain of 1310%. However, because of the experimental set up of this thesis, the maximum strain level is 830%.

The strain distribution along the membrane is not uniform. Both the FEA results and the experimentally obtained values show that the center of the membrane is dominated by tensile forces (positive values), and at the clamped edges of the membrane there are both tensile and contractile forces. The tensile forces are in the radial direction, and the contractile forces are in the circumferential direction. . Figures 6.1, 6.2, represent the diagrams of the strain distribution.

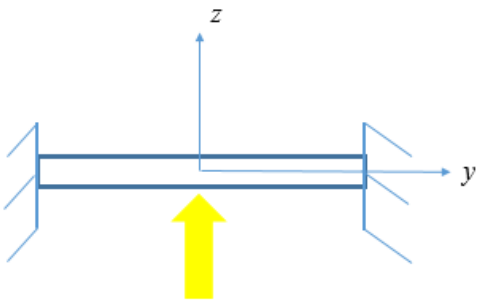

Figure 6.1 Pre-stretched membrane.

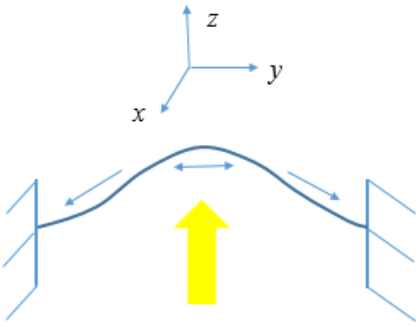

Figure 6.2 Strain distribution according to both the FEA and the experimental analysis

A strain of 20% at the center of the membrane was found experimentally and was confirmed using the Equation 3.1. This specific value was used because according to Ogawa et al., 29% is "the contraction rate in the vertical direction" [12] of the suprapubic region produced when a person is seating. The suprapubic region is located in between the navel and the pubic area. This area is of great interest since this is a common spot where stretch marks develop. The strain values vary depending on the region of the body. For example, the usually observed values in the upper body are between 5% and 8% (arms, shoulders, and chest) [12].

The main function of human dermal fibroblasts is to produce the ECM fibrous components, like collagen and elastin. Their healthy morphology is characterized by a flat, spindle shape, with clear and branched cytoplasm, and oval-shape nucleus. After one hour of stretch at 20% strain, the cell morphology changed. Most of the cells lost their elongated, flat morphology, and acquired a more rounded shape, with a less branched cytoplasm, and a non-distinguishable nucleus (Figures 5.5-5.10). The cell quantification (Tables 5.1 – 5.2) shows that the cells are dying as a function of strain; since cell viability is less than 50%. Therefore, cells sense the mechanical properties of the substrate/ECM and properly react to it by migrating, surviving, dying, among other responses.

From the results, it was also observed that after the applied stretch, the cells moved around the membrane. The angles of three cells before and after deformation were measured to quantify cell migration. The polar plots of the three respective cells were plotted. Cell 1 shows a bigger change in angles compared to cells 2 and 3, which leads to state that the applied force induced cell migration/mobility. However, this technique is not optimal to apply for this thesis because the cells need a marker in order to be identified

after the experiment is conducted. It is necessary a more in depth migration analysis to clearly define whether or not the cells follow both the circumferential and radial strain components as a guide for them to move.

Therefore, cell polarity was analyzed in order to quantify the morphological changes of the cells after deformation. Cell polarity refers to the healthy shape of fibroblasts characterized by an elongated body with branched cytoplasm. From experiment 1, three images were randomly selected from the same area before and after deformation. Lines were drawn through the cells with a polar shape and visible nucleus before deformation; after deformation, lines were drawn through the remaining polar cells. Based on images 5.15 – 5.21, there are less polar/elongated cells after the applied stretch. Confirming that cells change their morphology as a response to the mechanical forces of the ECM/substrate [1, 34].

CHAPTER 7

CONCLUSIONS

The stretching device designed for this thesis is a good model to study how multi-axial mechanical forces affect dermal fibroblasts, and hence scar formation in vitro. However, from the set of experiments, it is too early to conclude how stretch marks are formed. Although the mechanical simulation of severe skin stretching is obtained with the device, the 2D cell cultures do not properly represent the in-vivo state of the cells within the skin. Therefore, the results from a 2D culture could potentially differ from the results of a 3D cell culture. It is confirmed that the cells change their morphology and polarity as a function of applied mechanical strain, becoming rounded with a less branched cytoplasm and a darker and non-distinguishable nucleus after one hour deformation. Also, the cells move around the membrane as observed from all images in Chapter 5. However, the technique used to measure the angles is not optima to generate usable data. It is difficult to recognize and select the same cells from the same area before and after deformation. The polar plots were shown as a means of demonstrating the technique used to quantify cell mobility.

For future studies, the device must be modified to prevent the media to dry out for experiments longer than one hour. The device should also be re-designed so the experiments can be executed under the microscope allowing for life-time images. Specific selected cells must be marked, so they can be tracked and observed during the deformation. Proper analysis of protein synthesis before and after the deformation will help determine how much collagen and elastin fibers are being produced as a function of

mechanical strain. Moreover, 3D cell culture will be ideal using hydrogel matrices in order to closely resemble the in vivo structure of the skin. Since, the localized presence of steroid hormones are considered as a potential cause for stretch mark formation, future studies should include an analysis of how such hormones affect human dermal fibroblasts and their possible correlation with scar formation.

REFERENCES

1. Huang C, Miyazaki K, Akaishi S, et al. Biological effects of cellular stretch on human dermal fibroblasts. Journal of Plastic, Reconstructive & Aesthetic Surgery. 2013;66;12:351-61.

2. Pratsinis H, Dimozi A, Pilichos K, et al. Previous chronic exogenous glucocorticoid administration in vivo does not affect functional characteristics and cellular lifespan of human skin fibroblasts in vitro. Experimental Dermatology. 2011;20;6:529-31.

3. Slominski A, Zbytek B, Nikolakis G, et al. Steroidogenesis in the skin: implications for local immune functions. The Journal of steroid biochemistry and molecular biology. 2013;137:107-23.

4. Guo S, Dipietro LA. Factors affecting wound healing. Journal of dental research. 2010;89;3:219-29.

5. Bayat A, McGrouther DA, Ferguson MWJ. Skin scarring. BMJ. 2003;326.

6. Ferguson MWJ, O'Kane S. Scar–free healing: from embryonic mechanisms to adult therapeutic intervention. Philosophical Transactions of the Royal Society of London Series B: Biological Sciences. 2004;359;1445:839-50.

7. Garcia Hernandez JA, Madera Gonzalez D, Padilla Castillo M, et al. Use of a specific anti-stretch mark cream for preventing or reducing the severity of striae gravidarum. Randomized, double-blind, controlled trial. International journal of cosmetic science. 2013;35;3:233-7.

8. McIntire BJ, Pine H, Quinn FB, et al. Wound healing - scar minimization. The University of Texas Medical Branch. Editor. 2014: 1-7.

9. Evans ND, Oreffo ROC, Healy E, et al. Epithelial mechanobiology, skin wound healing, and the stem cell niche. Journal of the Mechanical Behavior of Biomedical Materials. 2013;28:397-409.

10. Enoch S, Leaper DJ. Basic science of wound healing. Surgery (Oxford). 2005;23;2:37-42.

11. Xia W, Hammerberg C, Li Y, et al. Expression of catalytcally active matrix metalloproteinase-1 in dermal fibroblasts induces collagen fragmentation and functional alterations that resemble aged human skin. Aging Cell. 2013;12;661-671.

12. Ogawa R, Okai K, Tokumara F, et al. The relationship between skin stretching/contraction and pathologic scarring: the important role of mechanical forces in keloid generation. Wound Repair Regen. 2012;20;2;149-57.

13. Gauglitz GG, Korting HC, Pavicic T, et al. Hypertrophic scarring and keloids: pathomechanisms and current and emerging tratments strategies. Molecular Medicine. 2011;17,1-2:113-125.

14. Viennet C, Bride J, Armbruster V, et al. Contractile forces generated by striae distense fibroblasts embedded in collagen lattices. Arch Dermtol Res. 2005;297;1;10-7.

15. Mohamed L, Elsaie ML, Leslie S et al. Striae distensae (stretch marks) and different modalities of therapy: an update. Dermatologic Surgery. 2009.

16. Plastic surgery statistics report. 2013. Available from: http://www.plasticsurgery.org/news/plastic-surgery-statistics/2013.html. [Accessibility verified May 9, 2015]

17. DermNet NZ. Stretch marks (striae). Available from: http://www.dermnetnz.org/. [Accessibility verified May 9, 2015]

18. Wound management innovation cooperative research centre - a new model for inter-disciplinary wound research. International Wound Journal. 2012;111-114

19. Girardeau S, Mine S, Pageon H, et al. The Caucasian and African skin types differ morphologically and functionally in their dermal component. Exp Dermatol. 2009;18;8:704-11.

20. Venus M, Waterman J, McNab I. Basic physiology of the skin. Surgery (Oxford). 2011;29;10:471-4.

21. Alberts B, Johnson A, Lewis J, et al. Molecular biology of the cell. 5th ed. New York, New York: Garland Science, Taylor & Francis Group, 2008.

22. Thome CH, Bauer BS. Tissue expansion in Grabb and Smith's Plastic Surgery. Lippincott Williams & Willkins. 2007:84-90

23. Zollner AM, Buganza A, Gosain AK, et al. Growing skin: tissue expansion in pediatric forehead reconstruction. Biomechanics and modeling in mechanobiology. 2012;11;6:855-67.

24. L'oreal. The hypodermis. Available from: http://www.skin-science.com/_int/_en/topic/topic_sousrub.aspx?tc=SKIN_SCIENCE_ROOT%5EAN_ORGAN_REVEALED%5ETHE_HYPODERMIS&cur=THE_HYPODERMIS. [Accessibility verified May 9, 2015]

25. Mazyala EJ. Dermal fibroblasts: a histologcial and tissue culture study. University of Stellenbosch: Faculty of Health Sciences. 2008;256.

26. Ingber DE. Cellular mechanotransduction: putting all the pieces together again. The FASEB Journal. 2006;20.

27. Eckes B, Nischt R, Krieg T. Cell-matrix interactions in dermal repair and scarring. Fibrogenesis & tissue repair. 2010;3:4.

28. Gallagher AJ, Anniadh AN, Bruyere K, et al. Dynamic tensile properties of human skin. IRCOBI Conference. 2012:494-502

29. Edsberg LE, Mater RE, Baier RE, et al. Mechanical characteristics of human skin subjected to static versus cyclic normal pressures. Journal of Rehabilitation & Development. 1999;36;2.

30. Morrison III B, Meaney DF, McIntosh TK. Mechanical characterization of an in vitro device designed to quantitatively injure living brain tissue. Annls of Biomedical Engineering. 1998;26:381-90.

31. Shao Y, Tan X, Novitski R, et al. Uniaxial cell stretching device for live-cell imaging of mechanosensitive cellular functions. The Review of scientific instruments. 2013;84;11:114304.

32. Lee AA, Delhass T, Waldman LK, et al. An equibiaxial strain system for cultured cells. American Journal of Physiology. 1996;271:1400-8.

33. Sotoudeh M, Jalali S, Usami S, et al. A strain device imposing dynamic and uniform equi-biaxial strain to cultured cells. Annals of Biomedical Engineering. 1998;26:181-9.

34. Wang D, Xie Y, Yuan B, et al. A stretching device for imaging real-time molecular dynamics of live cells adhering to elastic membranes on inverted microscopes during the entire process of the stretch. Integrative biology: quantitative biosciences from nano to macro. 2010;2;5-6:288-93.

35. Kanazawa Y, Nomura J, Yoshimoto S, et al. Cyclical cell stretching of skin-derived fibroblasts downregulates connective tissue growth factor (CTGF) production. Connective tissue research. 2009;50;5:323-9.

36. Dickson MG, Sharpe DT, Dickson WA, et al. Breast reconstruction by tissue expansion. Annals of the Royal College of Surgeons of England. 1986;68.

37. Magou GC, Guo Y, Choundhury M, et al. Engineering a high throuhput axon injury system. The journal of Neurotrama. 2011;28:2203-2218.

38. Ugural AC. Stresses in plates and shells. 2nd ed. The McGraw-Hill Companies, Inc, 1999.